Stony Brook University

Oceanic and atmospheric influences on the interannual variability of the Madagascar phytoplankton bloom

A Thesis Presented
by

Lindsay Roupe

to
The Graduate School
in Partial Fulfillment of the
Requirements
for the Degree of

Master of Science

in

Marine Science

Stony Brook University

December 2014

Stony Brook University

The Graduate School

Lindsay Roupe

We, the thesis committee for the above candidate for the

Master of Science degree, hereby recommend

acceptance of this thesis.

Kamazima Lwiza – Thesis Advisor
Associate Professor, School of Marine and Atmospheric Sciences

Bob Wilson – Second Reader
Associate Professor, School of Marine and Atmospheric Sciences

Sultan Hameed – Third Reader
Professor, School of Marine and Atmospheric Sciences

This thesis is accepted by the Graduate School

Charles Taber
Dean of the Graduate School

Abstract of the Thesis

Oceanic and atmospheric influences on the interannual variability of the Madagascar phytoplankton bloom

by

Lindsay Roupe

Master of Science

in

Marine Science

Stony Brook University

2014

Approximately every other year during the austral summer a larger phytoplankton bloom propagates off of the southeast tip of Madagascar. The cause of the interannual variability of this distinct oceanic feature remains unclear, so here we improve the analysis of the interannual variability of the bloom with a longer ocean color dataset, re-examine the existing mixed layer depth and iron fertilization hypotheses formerly used to explain bloom formation and analyze the variability in the larger ocean-atmosphere system in the region in relation to bloom formation. To resolve the forcings on the bloom, relevant satellite and reanalysis data were examined using principal component and wavelet analyses to tease out the dominant spatial and temporal patterns of variability. Composite maps were also created to examine how the physics evolves differently in bloom years compared to non-bloom years before and during bloom formation.

The dominant periods of variability in chlorophyll concentration data are 2- and 4-years, which are also present in other oceanic and atmospheric variables in this region. Neither of the existing hypotheses of mixed layer depth and iron fertilization was supported by this research. The mixed layer depth hypothesis is discounted by the presence of a shallower mixed layer depth, Chl correlations with higher SSTs and weaker winds during the time of bloom formation and the iron fertilization hypothesis was also not supported because of the correlation between anomalously lower precipitation rates and Chl and lack of evidence in sea surface salinity data. Instead, an alternative hypothesis is presented based on the existence of a biennial ocean-atmosphere mechanism in the Indian Ocean controlled by the upper ocean heat content and zonal surface winds. The sea surface temperature anomalies in the greater Madagascar region indicate that temperatures are cooler going into austral summer, combined with weaker winds, which induces lower surface thermal fluxes. The lower cloud cover associated with lower thermal fluxes allows a larger amount of photosynthetically active radiation (PAR) to reach the upper ocean and encourage phytoplankton growth. The increase in eastward flow in surface currents supports the propagation of the bloom, and the phytoplankton follow the movement of the eddy field including

both cyclonic and anti-cyclonic eddies. This mechanism is represented by anomalies in sea surface temperatures, zonal winds, precipitation rates, PAR, surface thermal radiation and, lastly, chlorophyll concentrations that act on an approximate 2-year timescale. However, this research does not explain the role of nutrients in the bloom, which were hypothesized to be regulated by the mixed layer depth. This conceptual framework based on statistical relationships and dominant variability in the oceanic and atmospheric fields over Madagascar sets the foundation of an alternative hypothesis to bloom development and an improved understanding of the ocean-atmosphere interactions in this region.

TABLE OF CONTENTS

ABSTRACT. iv
LIST OF FIGURES. vii
LIST OF TABLES. x
ACKNOWLEDGEMENTS. xi
THESIS: Oceanic and atmospheric influences on the interannual variability of the Madagascar phytoplankton bloom. 1
1. Introduction. 1
2. Data & Methods. 3
3. Results. 5
3.1 Bloom Characteristics. 5
3.2 Interannual variability of the phytoplankton bloom. 6
3.3 Oceanic and atmospheric variability in the Madagascar region. 7
3.4 Correlation Maps. 9
3.5 Composite analysis. 11
3.5.1 Oceanic and atmospheric variability in bloom region. 11
3.5.2 Variability in surface ocean circulation. 13
3.5.3 Atmospheric variability over Madagascar. 13
3.5.4 Spatial patterns between fields. 13
4. Discussion. 14
4.1 Re-visiting the mixed layer depth hypothesis. 14
4.2 Re-visiting the iron fertilization hypothesis. 16
4.3 Dipole mode in ocean-atmosphere system over Madagascar. 17
4.4 Dipole mode versus El-Nino Southern Oscillation. 19
4.5 Conceptual Diagram. 19
5. Conclusion. 22
FIGURES. 24
REFERENCES. 46

LIST OF FIGURES

1. Spatially-averaged Chl concentrations (mg m^{-3}) from January-April of bloom years (1999, 2000, 2002, 2004, 2006, 2008, 2012). The area of highest concentrations is outlined in black (22-31°S, 49-62°E) and is defined as the most common bloom region. 24

2. Composite maps constructed for a) December, b) January, c) February and d) March of the differences in Chl concentration anomalies (mg m^{-3}) between bloom (1999, 2000, 2002, 2004, 2006, 2008, 2012) and non-bloom years (1998, 2001, 2003, 2005, 2007, 2009, 2010, 2011). 25

3. Normalized time series of Chl concentrations spatially-averaged over the most common area of bloom formation southeast of Madagascar (22-31°S, 49-62°E). The largest peaks indicate bloom years. 26

4. The first mode a) eigenvector and b) normalized principal component time series in Chl concentration data over the bloom region from principal component analysis, representing 44% of the variability in the data. 27

5. a) Time-period plot of the dominant mode of variability from PCA, where color bar represents the power at each time-period point and b) the power sum from the wavelet showing overall dominant periods. 28

6. Power sums from the first mode principal component time series of zonal winds, precipitation rates, photosynthetically active radiation (PAR), mixed layer depth (MLD), SSTs and surface thermal radiation over the Madagascar region. The yellow bar represents the time period 22-26 months for comparison. Data were lopassed with a recursive Butterworth filter cut off at 70 months and power sums were normalized. . 29

7. The first mode a) eigenvector and b) normalized principal component in zonal wind data over the Madagascar region from principal component analysis, representing 40.6% of the variability in the data. 30

8. The first mode a) eigenvector and b) normalized principal component in precipitation rate data over the Madagascar region from principal component analysis, representing 20.1% of the variability in the data. 31

9. The first mode a) eigenvector and b) normalized principal component in precipitation rate data over Madagascar from principal component analysis, representing 35.5% of the variability in the data. 32

10. The first mode a) eigenvector and b) normalized principal component in photosynthetically active radiation data over the Madagascar region from principal component analysis, representing 18.7% of the variability in the data. 33

11. The first mode a) eigenvector and b) normalized principal component in mixed layer depth data over the Madagascar region from principal component analysis, representing 33.7% of the variability in the data. 34

12. The first mode a) eigenvector and b) normalized principal component in sea surface temperature data over the Madagascar region from principal component analysis, representing 37.9% of the variability in the data. 35

13. The first mode a) eigenvector and b) normalized principal component in surface thermal radiation data over the Madagascar region from principal component analysis, representing 25.3% of the variability in the data. 36

14. Power spectrums of the first and second modes of variability in surface thermal radiation data in the Madagascar region from PCA. 37

15. The second mode a) eigenvector and b) normalized principal component in surface thermal radiation data over the Madagascar region from principal component analysis, representing 18.1% of the variability in the data. 38

16. Correlation maps between the first mode PC time series in Chl data with normalized time series of a-c) zonal wind data, d-f) PAR data, g-i) MLD data and j-l) precipitation rate data at 2-month, 1-month and 0-month lags, respectively. Correlations with magnitude greater than +/-0.147 for zonal wind, +/-0.172 for PAR, +/-0.159 for MLD and +/-0.147 for precipitation rate were determined to be significant at the 95% confidence level. 39

17. Correlation maps between the first mode PC time series of PAR with normalized time series of a) zonal wind, b) surface thermal radiation and c) precipitation rate data. Correlations with magnitude greater than +/- 0.16 were determined to be significant at the 95% confidence level. 40

18. Composite maps constructed for December through March representing the difference in anomalies between bloom and non-bloom years for a-d) Chl concentrations, e-h) photosynthetically active radiation, i-l) precipitation rates, m-p) surface thermal radiation and q-t) zonal wind strength. Data has been normalized and climatology removed for all fields, then non-bloom anomalies are subtracted from bloom year anomalies. 41

19. Additional composite maps constructed for December through March representing the difference in anomalies between bloom and non-bloom years for a-d) sea surface temperatures and e-h) mixed layer depths. Data has been normalized and climatology removed for all fields, then non-bloom anomalies are subtracted from bloom year anomalies. 42

20. Composite maps of surface current vectors in a) bloom years, b) non-bloom years and c) the difference in the zonal component between bloom and non-bloom years. There

are little monthly differences from December to March, so only March maps are shown here.. 43

21. Nino3.4 index time series from 1998 to 2012. Solid circles mark bloom years and open circles mark non-bloom years for comparison. 44

LIST OF TABLES

1. Datasets that will be used in this research, including variables, time period, and resolution of those datasets. 45

ACKNOWLEDGEMENTS

The success of this thesis would not have been possible without the endless support I received from my thesis advisor, Dr. Kamazima Lwiza. He has had to deal with me finishing up my thesis remotely while moving locations twice, but he still made time for Skype calls. I would also like to thank my committee members Dr. Bob Wilson and Dr. Sultan Hameed, their statistical analysis classes helped lay the framework for this thesis. Lastly, I want to thank all of my peers at SoMAS who assisted in editing my work and just being there to lean on.

1. Introduction

Approximately every other year during the austral summer a large phytoplankton bloom propagates off of the southeast tip of Madagascar (Longhurst, 2001; Srokosz et al., 2004; Uz, 2007; Raj et al., 2010). The Madagascar phytoplankton bloom spans more than 1.7 million km^2 (Uz, 2007) and persists for 2-3 months before dying off, usually beginning between January and March and dissipating by the end of April (Longhurst, 2001; Uz, 2007). The mechanism behind bloom initiation has been attributed to the deepening of the mixed layer depth causing the entrainment of nutrients (Longhurst, 2001), iron fertilization by river runoff from Madagascar (Uz, 2007) and changes in current structure around the island (Raj et al., 2010). However, each of these theories has been criticized and still does not fully explain the interannual variability seen in bloom formation. This phytoplankton bloom is the strongest signal in ocean color imagery of interannual variability (Uz, 2007); however, the physical forcings need to be examined further to understand the cause of its specific interannual variability.

Longhurst (2001) was the first to describe this unique signal in ocean color imagery, which he attributed to the seasonal deepening of the mixed layer over a highly energetic eddy-field southeast of Madagascar, which acts to entrain nutrients in the photic zone from below. The presence of this eddy field would allow the bloom to propagate over great distances (Srokosz et al., 2004), supported by a high correlation between chlorophyll concentrations and sea surface height anomalies (Longhurst, 2001). The eddy field in this region is unique in that it includes both cyclonic and anti-cyclonic eddies that promote nutrient enhancement (Raj et al., 2010) by diffusing the phytoplankton against the mean flow (Srokosz et al., 2004). The eddy field varies seasonally where it is continuous during the austral summer and is weakened or not present during other seasons, consistent with the timing of bloom formation (Raj et al., 2010). The deepening of the mixed layer is attributed to strong southeast trade winds, which were anomalously weak in 1998 following a Niño event, resulting in the absence of bloom formation.

During the period of Longhurst's analysis (1998-2001) the bloom only failed this once, however, Uz (2007) also showed it to fail in 2001, 2003 and 2005. Uz (2007) rejected the mixed layer depth hypothesis because Argo float data showed the development of the bloom in a shallow mixed layer over a strong pycnocline. Uz also showed that Chl concentrations were correlated with higher SSTs that peak before bloom initiation, which should be cooler if nutrient-rich colder waters are being entrained from below. NCEP reanalysis winds were also not correlated with Chl concentrations, discrediting the connection between increased southeast trade winds and increased Chl.

Following his critiques of the mixed layer hypothesis, Uz (2007) introduced an alternative hypothesis describing the influence of river runoff from Madagascar on nutrient enhancement and phytoplankton growth in the area south of Madagascar. Uz's iron fertilization hypothesis requires that increased precipitation occur over Madagascar, increasing micro-nutrient runoff in the form of iron into the nutrient-poor waters surrounding Madagascar. Uz offered this hypothesis to explain the correlation between the number of cyclone landings over Madagascar and bloom formation, and the absence of a correlation with any other physical parameter tested. Precipitation was found to be higher in austral summer over east Madagascar compared to austral winter (26 cm/month compared to 4 cm/month) (Raj et al., 2010). River runoff on this side of the island would be carried by the East Madagascar Current (EMC) to the southern tip of Madagascar where it would meet the eddy field.

However, Uz did not find a correlation between precipitation and Chl, which he argues is due to the inability of the dataset to capture cyclone events, represented by peaks in precipitation. The iron fertilization hypothesis was also questioned because of the formation of a bloom during 2005 when the number of cyclones that made landfall on Madagascar was low in comparison to other non-bloom years (Raj et al., 2010). Additionally, this hypothesis does not explain why the bloom does not occur directly off the coast of Madagascar but some distance east, which Uz attributes to unfavorable hydrographic conditions for diazotrophs in the region right off the coast.

The circulation around Madagascar would also have to support the movement of river runoff into the area of bloom formation south of Madagascar. During the austral summer, when bloom formation occurs, the East Madagascar Current (EMC) flows westward and the southern limb loops into the southern Mozambique Channel, allowing the current to abruptly shift from a narrow to wide shelf (Lutjeharms & Machu, 2000), promoting upwelling along the southern tip of Madagascar (DiMarco et al., 2000; Lutjeharms & Machu, 2000; Machu et al., 2002; Raj et al., 2010). During the austral winter, the current flows southwestward and joins the Agulhas Current without looping into the channel (Heywood & Somayajulu, 1997; Raj et al., 2010). The direction that the EMC takes south of Madagascar depends on both its speed and local winds, creating a weaker current in bloom years (Raj et al., 2010). Additionally, the eddy field changes seasonally, with a continuous chain of eddies that propagates eastward in austral summer that is absent or weak in other seasons. Eddies are also seen southwest of Madagascar and in the Mozambique Channel (Quartly & Srokosz, 2004; Raj et al., 2010), where increased Chl concentrations also occur during bloom formation.

Variability in light limitation could also influence bloom formation. Photosynthetically active radiation (PAR) is highest from December to February (55 Einstein/m^2/day) before most blooms form and does show a relationship with Chl concentrations (Raj et al., 2010). Bloom formation is thought to be initialized by *Trichodesmium*, nitrogen-fixing cyanobacteria that convert atmospheric nitrogen into nitrogen compounds, who prefer SSTs >25°C (Uz, 2007; Poulton et al., 2009; Raj et al., 2010). Increased insolation combined with increased precipitation would also increase stratification, encouraging *Trichodesmium* growth (Hansell & Feely, 2000).

Furthermore, because of the approximate 2-year period in the interannual variability in bloom formation, it is also important to consider the ocean-atmosphere biennial mechanism that exists in the larger Indian Ocean region. The biennial signal in the ocean-atmosphere system in this region is thought to be controlled by anomalies in SSTs and zonal winds, where one year experiences anomalously warm SSTs and stronger winds and the following year has cooler SSTs and weaker winds, acting on a biennial time scale (Meehl, 1993). SST anomalies across the equatorial Indian Ocean are represented by the Dipole Mode Index (DMI), which has a high correlation with zonal equatorial winds (R= 0.6) (Saji et al., 1999). Zonal surface winds have been cited as a potential physical contributor to bloom formation (Longhurst, 2001; Uz, 2007; Raj et al., 2010), where meridional winds are weak in this region and are considered insignificant in comparison to zonal winds (Longhurst, 2001). The biennial tendency in these fields is likely cause by internal coupled dynamics in this region (Barnett, 1983; Saji et al., 1999; Feng & Meyers, 2003; Yeo & Kim, 2013) and could influence bloom formation (Conversi & Hameed, 1997).

Because of the remaining inconsistencies in explanations of the 2-year signal in bloom initiation off of southeast Madagascar, the analysis of the interannual variability of the bloom is improved using a longer ocean color dataset, along with principal component and wavelet analyses aimed to tease out dominant patterns of variability. Additionally, the existing

hypotheses of mixed layer depth and iron fertilization are re-examined using satellite and reanalysis data. Lastly, the biennial tendency of the ocean-atmosphere system is examined in relation to bloom formation.

Central to the mixed layer depth hypothesis is the idea of the entrainment bloom, which involves the combination of a deepening mixed layer entraining nutrients from below and increasing irradiance to enhance phytoplankton growth (McCreary et al., 1996). Therefore, mixed layer depth (MLD), sea surface temperature (SST), zonal wind and PAR data are examined for their dominant patterns of variability in relation to bloom formation. Correlation maps between these fields and a time series of Chl data are created to examine spatial patterns in these correlations and composite maps are created representing the monthly time-averaged differences between bloom and non-bloom years in the individual fields.

To re-examine the iron fertilization hypothesis, precipitation rate data from the Tropical Rainfall Measuring Mission (TRMM) is examined using PCA, correlation maps and composite maps, because it is more representative of tropical regions compared to the CPC Merged Analysis of Precipitation (CMAP) pentad data that Uz (2007) used. Additionally, sea surface salinity (SSS) data from NASA's new Aquarius satellite are used to determine if anomalies are consistent with the hypothesis of river runoff into the area of bloom formation and surface ocean current data are examined to determine if there are differences in circulation patterns in bloom years compared to non-bloom years (Raj et al., 2010).

Furthermore, the biennial tendency of the ocean-atmosphere system in the tropical Indian Ocean is examined for relevance to bloom formation using zonal wind, surface thermal radiation (STR), SST, precipitation rate and PAR data. These data are examined over the Madagascar region for interannual variability using PCA and composite maps. Additionally, correlation maps are used to examine the influence of the individual fields on bloom formation. If the ocean-atmosphere biennial mechanism influences bloom initiation, then anomalies in the ocean-atmosphere system would influence irradiance and nutrient availability in connection with phytoplankton growth. Specifically, anomalies in zonal winds and SSTs would induce changes in surface thermal radiation fluxes and precipitation rates, which would control irradiance and mixed layer depth, therefore controlling phytoplankton growth.

Our analysis aims to improve the understanding of bloom variability in the Madagascar region and improve the analysis on existing hypotheses using longer, more accurate datasets, including mixed layer depth, iron fertilization and surface ocean circulation. Additionally, variability in the ocean-atmosphere system in the Indian Ocean can be examined using multiple oceanic and atmospheric data and tested for influence on bloom initiation. This research provides a conceptual framework that improves our understanding of the unique phytoplankton bloom that propagates southeast of Madagascar and ocean-atmosphere coupled dynamics in the Indian Ocean basin.

2. Data and Methods

Monthly, gridded chlorophyll concentration data comes from SeaWiFS (Sea-Viewing Wide Field-of-View Sensor) and MODIS (Moderate Resolution Imaging Spectroradiometer), which, when integrated, covers the time span 1998-2013 at 1/12°x1/12° resolution (http://gdata1.sci.gsfc.nasa.gov). The datasets were normalized before integrating, SeaWiFS covering 1998-2007 and MODIS 2008-2013. The two datasets agree well in reported chlorophyll concentrations (root-mean-square difference of 0.2

(http://modis.gsfc.nasa.gov/sci_team/meetings/200207/presentations/campbell.pdf). The area of common bloom formation is defined as 49-62°E, 22-31°S over southeast of Madagascar because most blooms form in this region (Figure 1). Other data used in this analysis include monthly datasets of surface wind and surface thermal radiation from ECMWF products (http://data-portal.ecmwf.int/data/d/interim_moda/), precipitation rate from TRMM (http://disc.sci.gsfc.nasa.gov/giovanni), PAR from SeaWiFS, mixed layer depth from the Geophysical Fluid Dynamics Laboratory (http://data1.gfdl.noaa.gov), surface ocean currents from OSCAR (http://www.oscar.noaa.gov/), SST from ERSSTv3 (http://www.ncdc.noaa.gov/data-access/marineocean-data/extended-reconstructed-sea-surface-temperature-ersst-v3b) and sea surface salinity from Aquarius (http://podaac.jpl.nasa.gov/SeaSurfaceSalinity/Aquarius). Additionally, time series of Niño3.4 (http://www.cpc.ncep.noaa.gov) and Dipole Mode (http://www.jamstec.go.jp) indices are examined for correlations with other fields and dominant periods of variability. (Note: See Table 1 for detailed descriptions of datasets)

To examine the relevance of different atmospheric and oceanic forces, principal component analysis (PCA) was performed on the datasets listed above for the Madagascar region. Precipitation data was also analyzed over Madagascar (44-50°E, 22-31°S) because of its relevance to the iron fertilization hypothesis. All datasets were filtered with a 70-month recursive Butterworth filter before PCA to focus on higher frequency variability relevant to bloom formation. PCA aims to find linear combinations that represent the greatest fraction of variability in the original dataset. This method is useful in identifying underlying trends in atmospheric and oceanic variables both spatially and temporally. PCA produces principal components (PCs) that represent fractions of the temporal variability in the data and eigenvectors that represent fractions of the spatial variability in a dataset by breaking up the covariance matrix into eigenvectors, E, and eigenvalues, λ (Wilks, 2011):

$$C = X' * X = E * \lambda * E' \quad (1)$$

Then by multiplying the original data by the eigenvectors, the principal components (U) can be determined:

$$U = X * E \quad (2)$$

The variance fractions explained by the principal components are tested for significance using North et al.'s rule (1982). The rule states that an eigenvalue is significant if its sampling error is smaller than the distance between itself and a neighboring eigenvalue, defined as $\sim\lambda(2/n)^{1/2}$ for eigenvalue λ. Only the principal components that are significant are considered in this analysis.

The principal component time series from PCA were examined using wavelet analysis (Grinsted et al., 2004) to determine the dominant periods of variability and the years where those signals occurred. Wavelet transforms allow for data to be broken up by their dominating frequencies and represented in a time-frequency domain, which allows analysis of variability in time, i.e. when a frequency is strong in a time series. Specifically, continuous-wavelet transforms (CWTs) are used here to analyze individual variables. A Matlab software package created by Grinsted et al. (2004) is used in this study to perform wavelet analyses. Grinsted et al. (2004)

state that the CWT of a time series is the convolution of the time-series data, X_n, can be represented as:

$$W_n^S(x) = \sqrt{\frac{\delta s}{s}} \sum_{n'=1}^{N} X_{n'} \psi_0[(n'-n)\frac{\delta t}{s}] \quad (3)$$

with a normalized and scaled Morlet wavelet, where ω_0 is the dimensionless frequency and η is dimensionless time:

$$\psi_0(\eta) = \pi^{-1/4} e^{i\omega_0 \eta} e^{-1/2\eta^2} \quad (4)$$

Finally, the wavelet power can then be determined as $|W_n^X(s)|^2$.

Using principal component and wavelet analyses, the first mode in chlorophyll data over the defined bloom region (49-62°E, 22-31°S) includes peaks in the years of bloom formation and a dominant period of variability of 2 years. The principal component time series of the first mode is used to create spatial correlation maps with other fields, correlating the time series at each grid point with the first mode PC time series in Chl concentrations. Monthly climatology was removed and the data were normalized for all fields. Correlations were tested for significance at a 95% confidence level.

Composite maps were constructed for relevant fields to examine their evolution before and during the initiation of blooms. Monthly composite maps were created for December to March by time-averaging the data separately for bloom and non-bloom years, then subtracting the two matrices to amplify to differences. Climatology was removed from the time series and the data were normalized before time-averaging. Climatology was not removed from surface ocean current data, so the vectors shown in the maps are representative of current direction.

3. Results

An analysis on datasets of Chl concentrations, zonal winds, precipitation rates, PAR, MLD, STR, SSTs and surface ocean currents reveals their dominant spatial and temporal patterns of variability and their relation to bloom formation. Principal component analysis reveals the dominant modes of variability in these fields both spatially and temporally in the form of eigenvectors and principal component time series, respectively. Wavelet analysis on the PC time series reveals the dominant periods present in these modes. Correlation maps of the PC time series of Chl concentrations and PAR with normalized data of other fields show spatially where they are most correlated. Finally, anomalies between bloom and non-bloom years are examined through composite maps created for December through March to determine how these fields evolve before and during bloom formation.

3.1 Bloom Characteristics

The Madagascar phytoplankton bloom typically encompasses the region southeast of Madagascar (~49°-62°E), but increased Chl concentrations also occur south and southwest of Madagascar and in the Mozambique Channel (Figure 1). To examine the month-to-month evolution of the bloom, composite maps were constructed using ocean color data from SeaWiFS and MODIS (Figure 2). In December, typically before the bloom begins, some increased Chl

concentrations are seen but a concentrated bloom has not yet developed. In January the bloom starts to form south to southeast of Madagascar and in the southern portion of the Mozambique Channel. In February the concentrations increase in the easternmost part of the bloom, which continues through March, while Chl concentrations in the Mozambique Channel and south of Madagascar have decreased.

The timing of bloom initiation and termination also varies, beginning as early as January and lasting until March or April, spanning anywhere from 2-4 months, based on spatially-averaged Chl concentrations over the most common area of bloom formation (22-31°S, 49-62°E) (Figure 3). The magnitude of Chl concentrations varies, with the highest spatially-averaged concentrations (>3.5 mg m^{-3}) in 1999, 2006 and 2008, respectively. The largest peaks coincide with the large austral summer blooms but an annual signal is also present in this region, representing the occurrence of a secondary, seasonal austral winter bloom.

3.2 Interannual variability of the phytoplankton bloom

Despite these temporal and spatial differences between blooms, the interannual variability between bloom and non-bloom years is the most striking. The blooms occur approximately every even-numbered year, including 1999, 2000, 2002, 2004, 2006, 2008, 2012 and 2014 (Note: 2014 data is not included in this analysis). The exceptions to this 2-year signal are 1998 when a bloom did not form, 1999 when a large bloom formed in an odd year and in 2010 when a bloom also did not form. A seasonal secondary bloom, occurring in austral winter, is also evident in the time series that has lower Chl concentrations than the summer bloom, which are not considered in this analysis.

The interannual variability in the phytoplankton bloom is examined further using principal component analysis on Chl data over the region southeast of Madagascar (22-31°S, 49-62°E). PCA allows us to objectively examine the variability in the chlorophyll data to determine when and where the patterns of variability are dominant. Before PCA, the data were filtered using a recursive Butterworth filter cut off at 70 months to focus on higher frequency variability. The first mode, which includes the austral summer blooms, represents 44% of the variability in Chl concentrations in this region. This mode attributes most of the variability (0.045) to the eastern portion of the bloom domain (~57°-62°E), the area furthest east from Madagascar (Figure 4a). The reconstruction of the time series from the first mode principal component shows a similar time series as the spatially-averaged time series mentioned above (R=0.80), with Chl peaks in the bloom years (Figure 4b). The secondary austral winter blooms have been minimized in this mode, with concentrations close to zero. A dominant 2-year signal is identified from the power sum of this mode, created from wavelet analysis, followed by a less dominant 4-year signal (Figure 5b). Furthermore, wavelet analysis shows that the 2-year signal is more present in the middle of the time series (2002-2010) and the 4-year signal is present in the beginning (1998-2004) (Figure 5a), although this signal is outside of the cone of influence.

Temporal and spatial variability is seen between blooms, including the timing of onset and termination of the bloom, longevity, and spatial coverage of enhanced Chl concentrations. However, the variability in the presence or absence of a bloom is the most intriguing. The dominant periods of variability in ocean color data, including the 2-year and 4-year periods, along with anomalies to the distinct 2-year period in 1998, 1999 and 2010. Although this pattern of interannual variability is well documented (Longhurst, 2001; Uz, 2007; Raj et al., 2010), the mechanisms involved in supporting or discouraging bloom initiation are still up for debate.

3.3 Oceanic and atmospheric variability in the Madagascar region

To understand the forcings on bloom initiation, relevant oceanic and atmospheric variables are examined for dominant patterns of variability. Zonal winds, precipitation rates, PAR, MLD, STR and SSTs in the Madagascar region were determined to also contain a 2-year signal in their first modes from PCA (Figure 6). These datasets were filtered using a recursive Butterworth filter cut off at 70 months before PCA to focus on higher frequency variability.

Zonal winds are important to bloom formation because it influences many of the parameters listed above, including cooling SSTs, mixing the surface ocean and encouraging air-sea fluxes. ERA Interim reanalysis zonal wind data over the Madagascar region contains a 2-year signal in the first mode of variability, but a 4-5 year signal is dominant (Figure 6). This mode accounts for 40.6% of the variability in the data and shows a dipole between north and southeast of Madagascar, with greater variability to the north of Madagascar (0.04 compared to -0.02) (Figure 7a). The principal component time series shows the largest negative peak before the 2008 bloom, one of the largest and earliest austral summer blooms (Figure 7b). Zonal winds in this region are dominated by westerlies, so variability indicates stronger or weaker westerlies. This principal component (PC) time series is negatively correlated with precipitation rates over Madagascar (R= -0.18) and the greater Madagascar region (R= -0.27) and positively correlated with PAR (R= 0.21) and SSTs (R= 0.1) with zero lag, indicating that weakened zonal winds are associated with higher precipitation rates, more PAR and higher SSTs. However, this mode is not correlated with the PC time series of Chl.

Precipitation rates are examined both over the greater Madagascar region and over the Madagascar land region. The land region is examined separately for patterns relevant to the iron fertilization hypothesis, which would require high precipitation rates to precede bloom development. Data from the Tropical Rainfall Measuring Mission are used here because they are better suited for regions in the tropics compared to CPC Merged Analysis of Precipitation (CMAP) data. Over the Madagascar region, the dominant mode includes both positive and negative variability between northeast and southwest of Madagascar, with the transition at the center of Madagascar (Figure 8a), describing 20.1% of overall variability. Precipitation rates based on the PC time series are anomalously negative before bloom initiation, with the largest magnitude in 1999, followed by 2001, 2002 and 2004, respectively (Figure 8b). This PC time series also shows a dominant approximate 2-year (28 month) period of variability (Figure 6) and is negatively correlated with Chl at 2- (R= -0.29) and 1- (R= -0.26) month lags, indicating that lower precipitation rates over the region around Madagascar precedes higher Chl concentrations associated with the bloom. At a 0-month lag, increased precipitation over the greater region surrounding Madagascar is highly negatively-correlated with lower PAR (R= -0.74).

The first mode of variability in precipitation rates over Madagascar, explaining 35.5% of the variability, is concentrated over the center region of Madagascar (0.04) (Figure 9a). The dominant period of variability in this PC time series is approximately 2 years (28 months), followed by a period of 4 years (Figure 6). The PC time series does show an increase in precipitation rates before some blooms, including 2004, 2008 and 2012, but even higher rates occur in non-bloom years (Figure 9b). This time series has a negative correlation (R= -0.13) with Chl at a 1-month lag, showing that a lower precipitation rate is associated with higher Chl, but the correlation is lower than with precipitation variability over the greater region. This mode is also negatively correlated with PAR (R= -0.20) and positively correlated with precipitation rates

over the Madagascar region (R= 0.36) at a 0-month lag, meaning a higher precipitation rate is associated with lower PAR.

PAR, the solar energy available for phytoplankton growth, is dominated by an approximate 2-year signal (28 months) in its first mode (Figure 6). This mode explains 18.7% of the variability and shows both positive and negative variability of approximately equal magnitude (+/- 0.02) (Figure 10a). This dipole exists between southwest and northeast of Madagascar, with negative variability in the area of bloom formation. Positive peaks in PAR are shown before most blooms, including 1999, 2002, 2004 and 2008, and PAR is anomalously negative in 2010, when a bloom did not form (Figure 10b). The first mode PC time series of PAR in the greater Madagascar region is positively correlated with Chl at 2- (R= 0.26) and 1-month (R= 0.18) lags.

The role of MLD in phytoplankton blooms is well-understood in biological theory, as the deepening of the mixed layer below a critical depth of PAR creates favorable conditions for phytoplankton growth. The first mode in MLD explains 33.7% of the variability and is dominated by positive variability (0.04-0.05) in the region east of Madagascar (Figure 11a). The principal component time series generally shows a shoaling of MLD in months leading up to bloom initiation (January-March), but these anomalies are small in comparison to anomalies throughout the rest of the time series (Figure 11b). This mode includes both a 2-year and 40-60-month period of variability of approximate equal magnitudes (Figure 6), but is not correlated with Chl. However, a deeper MLD is correlated with warmer SSTs at a 0-month lag (R= 0.19).

SSTs are examined because they reflect the deepening of the mixed layer, are influenced by cloud cover, and warmer SSTs can encourage growth in *Trichodesmium*, the nitrogen-fixing Cyanobacteria that are thought to trigger the bloom. Also, Uz (2007) used SSTs as one of the reasons Longhurt's (2001) hypothesis fails, because his analysis showed that SSTs peak after the bloom onset and Chl is associated with high SSTs, rather than low. The first mode in SSTs accounts for 37.9% of variability and includes a dominant approximate 2-year (28-month) signal, followed by a smaller 4-year signal (Figure 6). The variability is largest south of Madagascar and in the Mozambique Channel (0.10), encompassing the area of bloom formation (Figure 12a). The PC time series shows increasing SSTs following blooms, but the warmest SSTs are seen in non-bloom years, excluding 1999 (Figure 12b). This mode is correlated with Chl at a 2-month lag (R= 0.17), when increased Chl precedes increased SSTs.

STR is influenced by precipitation, winds and SSTs, which all act to either enhance or depress thermal energy transfer between the ocean and atmosphere. The first mode of STR explains 25.3% of the variability and shows a slight dipole between the northeast and southwest regions off of Madagascar (Figure 13a), with most of the variability occurring east of Madagascar (0.08). The principal component time series for the first mode shows the large negative peaks prior to bloom formation in 1999, 2000, 2002 and 2006, but there is also a large negative peak in 2011 (Figure 13b). This mode includes an approximate 2-year signal, although it is less dominant than a 40-month signal (Figure 6). The second mode (18.1% of total variability) does have a dominant approximate 2-year (28-month) signal (Figure 14) and contributes most of its variability (-0.08) to the region where blooms occur, including the southern Mozambique Channel and south and southeast of Madagascar, along with the Madagascar land region, and less positive variability north of Madagascar (Figure 15a). The strongest negative peaks in the PC time series sometimes coincide with bloom years, including 1999, 2002 and 2008 (Figure 15b), but there are also negative peaks in non-bloom years.

STR is correlated with Chl, zonal winds, precipitation rates, PAR and MLD. The first mode PC time series of STR and Chl are negatively correlated (R= -0.34) at a 2-month lag, which decreases in magnitude at a 1-month (R= -0.27) and is not significant at a 0-month lag. This mode in STR is also negatively correlated with PAR (R= -0.45) at a 0-month lag, indicating that a higher flux of thermal radiation is associated with less PAR. STR is positively correlated with precipitation rate both over the land (R= 0.47) and the greater region (R= 0.59) at a 0-month lag, along with SSTs (R= 0.16), indicating a higher thermal flux is associated with higher precipitation rates and warmer SSTs.

The second mode in STR shows correlations with zonal winds (R= 0.21), precipitation rates over land (R= -0.33), precipitation rates over the greater region (R= 0.29), PAR (R= -0.46), MLD (R= -0.26) and SSTs (R= -0.27) at a 0–month lag, but not with Chl. Correlations with precipitation rates over land and SST have an opposite sign with the 2nd mode, indicating that a higher thermal flux is correlated with a lower precipitation rates over Madagascar and cooler SSTs, but is still associated with higher precipitation rates over the greater Madagascar region and less PAR. The first modes in zonal wind, PAR and precipitation rate over the greater Madagascar region and the 2nd mode in STR all show spatial variability patterns that include a dipole structure with the transition over Madagascar, indicating the influence of this land mass on the variability in these fields. The southern portion of the dipole includes the area of bloom formation south-to-southeast of Madagascar and the Mozambique Channel.

To summarize the correlations in PC time series, increased Chl concentrations are correlated with higher PAR, lower precipitation rates over the greater Madagascar region and lower STR fluxes at a 2-month lag and lower precipitation rate over Madagascar at a 1-month lag. At a 0-month lag, lower PAR is highly correlated with higher precipitation rates over the greater region (R= -0.74), and is also correlated with a lower precipitation rate over Madagascar, stronger westerlies and a lower STR flux. Additionally, stronger westerlies and a deeper MLD are correlated with warmer SSTs at a 0-month lag. Finally, following increased Chl concentrations, warmer SSTs are correlated with Chl at a 2-month lag (R= 0.17).

Interestingly, MLD is not correlated with any of the fields above at 0-2 month lags besides SSTs, but correlations are seen at 5-6 month lags. When higher STR fluxes and higher precipitation rates over the greater region precede MLD by 6 months, they are correlated with a shallower MLD (R= -0.22 and R= -0.24, respectively). At a 5-month lag, higher precipitation rates over Madagascar are also correlated with a shallower MLD (R= -0.20), changes in precipitation preceding MLD. Then moving 6 months ahead, MLD preceding, a more shallow MLD is correlated with higher Chl concentrations (R= -0.18). The 6-month difference in correlations between MLD and STR, precipitation rates and Chl concentrations indicates that there could be 6-month forcing that pre-conditions the austral winter for bloom formation.

3.4 Correlation Maps

Correlation maps were constructed to compare variability in Chl with PAR, zonal winds, MLD and precipitation rates. Correlations were calculated with 0-, 1- and 2-month lags to examine spatial variations in these fields leading up to bloom formation. Maps were also created for PAR with zonal winds, STR and precipitation rates at a 0-month lag to determine how these fields vary together spatially. Correlations were tested for significance at a 95% confidence level and determined to be significant when the magnitude is greater than +/- 0.16.

The correlation maps of zonal winds show both positive and negative correlations with Chl at 2- to 0-month lags, with stronger negative correlations (R~ -0.3 versus 0.15). The negative correlations start on the east coast of Africa at a 2-month lag (Figure 16a) and transition east to northeast of Madagascar at a 1-month lag, indicating a movement of weaker westerlies correlated with increased Chl (Figure 16b). At the 0-month lag negative correlations are shown over Madagascar and east of Madagascar (Figure 16c). Positive correlations are shown south of Madagascar, in the Mozambique Channel and further north of the negative correlations. The largest positive correlations are seen in the southern Mozambique Channel at a 2-month lag that decrease moving from the 2- to 0-month lags, along with the positive correlations south of Madagascar. North of Madagascar positive correlations get larger and spread further west as lags decrease.

PAR is also both positively and negatively correlated with Chl in the Madagascar region. Correlations between these two fields reach magnitudes > +/-0.35 at a 0-month lag. At a 2-month, correlations are relatively low but slightly positive and negative in the area of bloom propagation and larger positive correlations are seen northeast of Madagascar (Figure 16d). At a 1-month lag, positive correlations are still present northeast of Madagascar and positive correlations appear in the area of bloom formation, including the southern Mozambique Channel and southeast of Madagascar (Figure 16e). At a 0-month lag, positive correlations are larger in magnitude (R~ 0.3) southeast of Madagascar and are also higher further east from 55°E to 64°E (Figure 16f). PAR plays an important role in the development of phytoplankton blooms, providing the solar energy needed to promote phytoplankton growth, so positive correlations between these two fields in the area of bloom formation is expected.

MLD plays an important role in the entrainment theory of bloom formation because it must be deep enough to entrain nutrients from below. However, correlation maps with mixed layer depth were the lowest of all the fields that were correlated, with maximum positive correlations of R= 0.2 and negative correlations of R= -0.18. At a 2-month lag, non-significant low negative correlations (R= -0.05) are seen in the Mozambique Channel and southeast of Madagascar in the area of bloom formation and positive correlations (R=0.15) northeast of Madagascar (Figure 16g). Correlation maps at 1- and 0-month lags are spatially similar, with negative correlations (R= -0.05-0.15) in the southern Mozambique Channel and northeast of Madagascar (Figures 16h-i). Additionally, positive correlations (R = 0.15-0.2) are shown east of Madagascar, which shift further south at a 0-month lag, into the area of bloom formation (Figure 16i).

Correlations between Chl concentrations and precipitation rates show spatial similarity to correlations with PAR. Positive correlations (R= 0.1-0.3) exist in the southern Mozambique Channel and south of Madagascar and negative correlations (R= -0.1-0.3) are seen over east Africa and north of Madagascar at a 2-month lag (Figure 16j). Transitioning to a 1-month lag, correlations are spatially similar to the 2-month lag map, but negative correlations (R= -0.3) are now over Madagascar (Figure 16k). At a 0-month lag, there are positive correlations north and southeast of Madagascar (R= 0.1-0.3) and the negative correlations (R= -0.2) over Madagascar remain (Figure 16l).

In addition to understanding the direct forcings on the phytoplankton bloom, we also want to understand the atmospheric forces on these parameters that would create a 2-year signal. Correlations between the dominant mode of variability in PAR with zonal winds, MLD and precipitation rates are examined to determine the correlations with increased PAR in this region

at the time of bloom formation. Correlations between these fields of magnitude greater than +/- 0.16 are significant at the 95% confidence level.

Increased PAR is negatively correlated (R= -0.4-0.5) with zonal wind strengths over Madagascar, southern Mozambique Channel and east and southeast of Madagascar, which would indicate weaker westerlies (Figure 17a). PAR and zonal wind are positively-correlated (R= 0.3) over east Africa, north of Madagascar and the northern Mozambique Channel. Correlations between PAR and STR are negative over the southern Mozambique Channel and south and southeast of Madagascar and positive northeast of Madagascar (Figure 17b). The correlations between the first mode of variability in PAR with precipitation are also negative (R= -0.5) south of Madagascar and positive (R= 0.5) north of Madagascar (Figure 17c), but the dipole is situated southwest to northeast instead of directly north and south.

Therefore, in the area of bloom formation southeast of Madagascar, increased PAR is correlated with weaker westerlies, lower surface thermal fluxes and lower precipitation rates. From the correlation maps with Chl data, increased chlorophyll concentrations are correlated with increased PAR, a deeper MLD and a higher precipitation rate over the area of bloom formation, but show much less spatial coherence. Additionally, correlations between PAR and zonal winds, STR and precipitation rates show a similar dipole structure between north and south of Madagascar that is also shown in the first mode of PAR from PCA. This dipole is also slightly evident in the correlation maps between Chl and PAR and precipitation rates at 2- and 1-month lags.

3.5 Composite analysis

The ocean-atmosphere connections are further examined using composite maps of anomalies between bloom and non-bloom years. Bloom years are defined as years when the spatially-averaged chlorophyll concentration anomaly is >=0 over the bloom region, including 1999, 2000, 2002, 2004, 2006, 2008 and 2012. The composite maps show the spatial anomalies in ocean and atmospheric variables averaged over all bloom years with spatially-averaged anomalies from non-bloom years (1998, 2001, 2003, 2005, 2007, 2009, 2010 and 2011) subtracted to amplify differences. There are distinct spatial pattern differences between bloom and non-bloom years in the relevant fields of PAR, precipitation rates, STR, zonal winds, SSTs, MLD and surface ocean current circulation. By examining how these variables evolve spatially in bloom years compared to non-bloom years, local variability relevant to bloom initiation can be resolved.

3.5.1 Oceanic and atmospheric variability in bloom region

During the Madagascar phytoplankton bloom increased Chl concentration anomalies are seen southwest to southeast of Madagascar, and sometimes in the Mozambique Channel. In December, there are only small anomalies between bloom and non-bloom years in the region surrounding Madagascar (Figure 18a), then moving into January, when blooms begin to form, increased Chl anomalies are seen south and southeast of Madagascar and in the southern Mozambique Channel (Figure 18b). In February, positive Chl concentration anomalies have peaked over southeast of Madagascar, but are still present in the Mozambique Channel and south of Madagascar and have developed further southwest of Madagascar (Figure 18c). By March,

positive Chl concentration anomalies have decreased in magnitude south and southwest of Madagascar and in the channel, but are still prominent to the southeast (Figure 18d).

In December of bloom years, before bloom initiation, PAR is lower over the area of bloom formation, including the Mozambique Channel and south and southeast of Madagascar, and higher north and east of Madagascar (Figure 18e). Precipitation rate anomalies are spatially similar to PAR, but with higher rates over the southern portion of the channel and south and southeast of Madagascar and lower rates north of Madagascar (Figure 18i). STR also shows a similar spatial structure to PAR and precipitation rate, with higher fluxes in the area of bloom formation and lower rates north (Figure 18m). Zonal wind strength is higher over the channel and east and southeast of Madagascar before bloom initiation (Figure 18q). SST anomalies are small in this month, with lower SST anomalies south of Madagascar and anomalously higher SSTs in the Mozambique Channel (Figure 19a). MLD is the deepest south of Madagascar in December and is slightly shallower east of Madagascar (Figure 19e).

In January, when the bloom is beginning to develop, PAR is high around Madagascar and southeast of Madagascar and slightly lower in the lower Mozambique Channel and southwest of Madagascar (Figure 18f). Precipitation anomalies are a mix of higher and lower rates with higher rates concentrated northeast of Madagascar and lower rates southeast of Madagascar (Figure 18j). STR anomalies are relatively small in January with slightly higher fluxes southeast of Madagascar and lower fluxes east and southeast of Madagascar (Figure 18n). Zonal wind strength has changed patterns showing weaker winds over southeast of Madagascar and stronger winds over the Mozambique Channel (Figure 18r). SSTs are lower south of Madagascar and even lower east of Madagascar (Figure 19b). MLD is deeper around Madagascar and east of Madagascar and slightly shallower southwest and southeast of Madagascar (Figure 19f). Some spatial similarities are seen here between PAR and MLD where the higher PAR around Madagascar is also where MLD is deeper and where there is lower PAR southwest of Madagascar there is also a shallower MLD.

By February, when Chl concentrations have peaked southeast of Madagascar, PAR is lower south of Madagascar and in the channel and higher east and northeast of Madagascar (Figure 18g). Precipitation rates are lowest east of Madagascar and higher in the Mozambique Channel and south of Madagascar (Figure 18k), where Chl concentrations have decreased. STR is lower east of Madagascar and higher in the channel and south and southwest of Madagascar (Figure 18o). Zonal wind strength is weakest in the area of bloom formation during this month, in the area of the higher Chl concentrations, and strongest over the Mozambique Channel and south of the weaker winds (Figure 18s). SSTs are the lowest southeast of Madagascar during this month and are also low in the northern areas surrounding Madagascar (Figure 19c). MLD anomalies are small in this month with slightly shallower depths south of Madagascar and slightly deeper east of Madagascar (Figure 19g).

In March, when Chl concentrations are still concentrated southeast of Madagascar and have decreased in the channel and southwest of Madagascar, PAR is anomalously higher over south of Madagascar and the channel (Figure 18h). Precipitation rates are scattered but show lower rates south of Madagascar and east of Madagascar, with some higher rates mixed in southeast of Madagascar (Figure 18l). STR anomalies are relatively small, with higher STR southeast of Madagascar and lower east of Madagascar (Figure 18p). Zonal wind strength is still anomalously lower east and southeast of Madagascar during this month, but has increased from February, while zonal wind strengths remain higher in the channel and further south of the weak winds, again of smaller magnitude (Figure 18t). SSTs have become anomalously high south of

Madagascar by March and remain anomalously cooler around northern Madagascar (Figure 19d). This transition from anomalously low to high SSTs occurs after bloom formation, corresponding to the positive correlation between the PC time series of these fields at a 2-month lag. Lastly, MLD is anomalously shallow southwest of Madagascar and further southeast and deeper east of Madagascar and in the northern Mozambique Channel (Figure 19h).

3.5.2 Variability in surface ocean circulation

Surface ocean currents also evolve differently in bloom years compared to non-bloom years. In general, surface ocean circulation shows westward flow moving towards Madagascar, namely the South Equatorial Current (SEC), which splits into the north and south components of the East Madagascar Current (EMC) upon encountering the island at approximately 18°S (Lutjeharms, 2006). The northern component increases in strength when moving around the north tip of the island while the southern component shows both westward and eastward propagation around the southern tip of Madagascar. In bloom years, currents moving east away from the southern tip of Madagascar are stronger and propagate further east in December through March of bloom years (Figure 20a) and westward propagation is weaker compared to non-bloom years (Figure 20b). This difference is shown to be dominant in the zonal component of current speeds (Figure 20c), with eddy variability.

3.5.3 Atmospheric variability over Madagascar

Variability over Madagascar is examined separately to determine if anomalies in the atmosphere over the island could encourage iron fertilization via river runoff. Over Madagascar, in December of bloom years, precipitation rates are slightly higher over the southern region (Figure 18i) and zonal wind strengths are anomalously strong (Figure 18q). These differences occur in the month preceding the initiation of the bloom and seem to represent different dynamics than the following January-March composite maps. A lower precipitation rate is seen over central Madagascar in January (Figure 18j), then precipitation rates are slightly higher over northern and lower over southern Madagascar in February and March (Figures 18k & 18l). Zonal wind strengths become anomalously weak in January (Figure 18r) and remain weak in February and March (Figures 18s & 18t). STR, which is correlated with precipitation rates and reflects changes in winds, shows anomalies of small magnitude that are almost zero in December and February (Figures 18m & 18o) and are slightly lower in January and March (Figures 18n & 18p).

3.5.4 Spatial similarity between fields

Overall, anomalies in PAR, precipitation rates and STR show spatial similarity, where higher PAR is associated with lower precipitation rates and lower STR fluxes. The amount of available PAR is affected by cloud cover, which would be associated with higher precipitation rates, and a lower STR flux means less thermal radiation is leaving the ocean. Anomalies in these fields around southern Madagascar in January are associated with increased Chl concentrations, where higher PAR, lower precipitation rates and lower STR fluxes occur where increased Chl concentrations are seen. Interestingly, in December, the patterns are the exact opposite, showing lower PAR, higher precipitation rates, and higher STR fluxes in the same region.

When examining PAR and MLD, the fields that are important to the entrainment theory, spatial patterns in anomalies are similar when considered with a lag. Where PAR is lowest in December southwest and southeast of Madagascar, MLD is shallower in the next month over the same region. The entrainment theory requires that enough PAR is available for phytoplankton to utilize and that MLD is deep enough to entrain nutrients from below. Similar spatial patterns are also seen in the fields of zonal winds, precipitation rates and STR in February when Chl concentrations are highest southeast of Madagascar. During this month, zonal wind strengths are the weakest, precipitation rates are lowest and STR is low compared to non-bloom years east of Madagascar. Surface ocean circulation is also weakest during this month in non-bloom years (not shown).

4. Discussion

When interpreting the results above, first the existing hypotheses are re-visited, including the mixed layer depth hypothesis introduced by Longhurst (2001) and the iron fertilization hypothesis introduced by Uz (2007). The mixed layer depth hypothesis is not supported by SST, MLD or zonal wind variability found in the analysis and the iron fertilization hypothesis is not supported by precipitation rate variability over Madagascar or SSS and surface ocean circulation around Madagascar. Additionally, the ocean-atmosphere biennial mechanism in the Indian Ocean is discussed in relation to the phytoplankton bloom. Due to the lack of sufficient evidence supporting either of the mixed layer depth or iron fertilization hypotheses from this analysis, a conceptual diagram is used to explain the correlations between the oceanic and atmospheric fields examined in the Madagascar region.

4.1 Re-visiting the mixed layer depth hypothesis

Longhurst (2001) introduced his mixed layer depth hypothesis to explain the spatial coherence of Chl concentrations and sea surface heights and the seasonal occurrence of bloom formation in austral summer every year except for 1998, over the time period of his analysis. Longhurst attributed this absence to a Niño year that contributed weak southeast trade winds instead of the strong winds required for bloom formation. This explanation is more commonly known as the entrainment theory, where nutrients are upwelled from deeper waters as surface irradiance penetrates deeper into the mixed water column, enhancing phytoplankton growth, which ends when irradiance decreases to above a critical depth. Cyclonic and anticyclonic eddies locally regulate the depth of the nutricline, effectively explaining the tight correlation between the two fields.

However, Uz (2007) showed that the bloom failed in multiple years after 1998, including 2001, 2003 and 2005. Additionally, using Argo float data in the bloom region from 2004, Uz found that the bloom developed in a shallow mixed layer over a strong pycnocline. He also found that increased Chl was correlated with high SSTs rather than lower temperatures representative of upwelling. These findings contradict the possibility of the entrainment hypothesis, which would require cooler, deeper mixed layer to be associated with bloom formation. Uz also did not find a correlation with the zonal component of NCEP reanalysis winds.

This analysis shows anomalously cooler SSTs before the bloom forms that increase in temperature as the bloom progresses until SSTs are anomalously high in March around the end

of the bloom. This is supported by the positive correlation (R= 0.17) between the PC time series between these fields at a 2-month lag, where increased Chl precedes warmer SSTs. The first mode of variability in SST data from PCA does show dominant variability in the area of bloom formation south of Madagascar that contains a dominant 28-month period, indicating that the higher SSTs do occur in the bloom region. The PC correlation results agree with Uz's analysis on Pathfinder reanalysis of AVHRR imagery data that Chl is correlated with higher SSTs, but anomalously cooler SSTs are shown to set up over the bloom region before bloom initiation.

We used data from NOAA's Geophysical Fluid Dynamics Laboratory to examine the mixed layer depth. Composite maps created from this data over the period of bloom formation show that the mixed layer is anomalously shallower in bloom years at the time of bloom formation, consistent with results from Argo floats. However, the mixed layer depth is deeper in December of bloom years, a month prior to bloom formation. This was not captured in the analysis of Argo data in 2004 because only the data around day 111 of 2004 is analyzed. The first mode in MLD data from PCA does not show spatial similarity to the area of bloom formation and is not correlated with Chl data. However, this mode is correlated with the first mode PC time series of SSTs, indicating that a deeper MLD is correlated with warmer SSTs and vice versa. This PC time series also does generally show a deepening mixed layer as Chl increases, but there are anomalies in 2002 where MLD peaks before Chl increases and then begins to decrease as Chl continues to increase. Due to the lack of consistency in MLD results, we cannot conclude if the mixed layer depth influences bloom formation in this region.

Uz (2007) used NCEP reanalysis wind data and did not find a correlation with Chl. In this analysis we used ECMWF wind data and still did not find a significant correlation between zonal wind and Chl concentrations, based on their dominant modes of variability. However, significant negative correlations are seen between the two fields in the correlation maps with zero lag. Increased Chl is correlated with weaker winds over Madagascar and east of Madagascar (R~ -0.30), which is the opposite of what is expected with the mixed layer depth hypothesis. Also, the correlation map between PAR and zonal wind shows high negative correlations over the area of bloom formation and over southern Madagascar (R~ -0.5), indicating a tight association between the two fields. PAR and Chl are correlated, shown in both in their PC time series and in their correlation maps, so the correlations between PAR and zonal winds in the area of bloom formation indicate that the Chl and zonal wind fields could be correlated through the PAR field. However, because the correlations between PAR and zonal wind are negative, they still do not support the mixed layer depth hypothesis, which would require stronger zonal winds to be correlated with higher PAR.

Overall, the results of this analysis support Uz's critiques of the long-standing mixed layer depth hypothesis, including the associations of increased Chl with warmer SSTs and a shallower mixed layer depth, and the lack of correlation between Chl and the zonal wind component. Even further, this analysis shows a correlation between increased Chl and weaker winds when examined spatially, contradicting the association between Chl and strong southeast trade winds indicative of the mixed layer depth hypothesis. However, the correlation between Chl concentrations and sea surface height cannot be overlooked, as the Chl concentrations clearly follow the distinct eddy circulation patterns and must be considered in explaining the cause of bloom formation.

4.2 Re-visiting the iron fertilization hypothesis

Uz's (2007) critiques of the long-standing mixed layer depth hypothesis left room for a new explanation on bloom formation southeast of Madagascar. He offered his iron fertilization hypothesis to explain correlations between increased Chl and cyclone landings on Madagascar, and the lack of correlation with any other physical parameter he tested. Uz supports this hypothesis by describing the ocean circulation around the island in support of iron runoff into the location of bloom propagation, i.e. the weakly westward flow east of Madagascar would keep the iron close to shore, then move southward with the lower portion of the EMC where it would meet the eddy field and spread laterally.

If his hypothesis were true, increased precipitation rates over Madagascar should be correlated with increased Chl, which he did not find in his analysis of CMAP pentad data. He shows that precipitation rates over Madagascar do not increase significantly with a cyclone landing and, therefore, must not be representative of cyclone events. For this analysis, we used TRMM data instead of CMAP, because it is more representative of regions near the tropics, and we have a longer dataset to work with. Our analysis of precipitation rates over Madagascar shows that the dominant mode of variability occurs over the central region and has a dominant 28-month period of variability. This mode is slightly negatively correlated with Chl (R= -0.13) when precipitation precedes Chl by one month, and is correlated with PAR (R= -0.20), STR fluxes (R= 0.47) and precipitation rates (R= 0.36) over the greater Madagascar region at zero lag. Correlation maps constructed for these fields also show negative correlations over Madagascar at a 1-month lag and zero lag. Composite maps show slightly higher precipitation rate anomalies in December and larger negative anomalies in January over central Madagascar. Therefore, the PC correlations indicate lower precipitation rates are associated with bloom formation and these anomalously lower precipitation rates occur over Madagascar in January, in conjunction with bloom initiation.

Raj et al. (2010) also questioned Uz's hypothesis because of the development of a bloom in 2005 when the number of cyclone landings was at its lowest. Uz also recognized the development of a small bloom at this time, but reported that it dissipated quickly. Our analysis does show that a bloom formed in 2005 but it contained lower Chl concentrations and did not cover the large spatial area other blooms covered. This bloom also begins in December, earlier than any other fully-developed bloom. Therefore, the forcings on this bloom could be different than the forcings on the blooms that usually occur in even-numbered years.

However, the most convincing evidence against the iron fertilization hypothesis comes from the new sea surface salinity (SSS) remote sensing data from NASA's Aquarius satellite. If nutrient runoff associated with cyclones causes bloom formation there should be a decrease in salinity in the waters southeast of Madagascar following a cyclone event that follows the path of bloom propagation. Composite maps of SSS data (not shown) show little differences between the bloom and non-bloom years where data is available and, in fact, shows slightly lower SSS in non-bloom years. Additionally, when examining the evolution of salinities around Madagascar from January to April, the low-salinity waters appear to enter the region from the northeast, where the South Equatorial Current enters the region, indicating that fresher water is a remote source rather than coming from the Madagascar land region.

Precipitation data from TRMM do not support the iron fertilization hypothesis because of the association of anomalously lower precipitation rates compared to non-bloom years. However, Raj et al. (2010) did find seasonal variability in precipitation over east Madagascar (47.5°-

52.5°E, 25°-12°S) where the amount of precipitation increases to 26 cm/month in the austral summer compared to 4 cm/month in the austral winter, which could influence iron runoff on a seasonal timescale. The absence of a signal in SSS data associated with bloom years is important because river runoff should be represented by lower salinities. However, Aquarius data has only been made available since August 2011, covering a single bloom year (2012) for comparison. Additionally, the monthly period of the data analyzed could smooth out signals in SSS from river runoff, which could be acting on shorter timescales following cyclone events.

4.3 Dipole mode in ocean-atmosphere system over Madagascar

A dipole mode with a biennial tendency has been documented in the ocean-atmosphere system of the tropical Indian Ocean (Barnett, 1983; Meehl, 1993; Saji et al., 1999; Yeo & Kim, 2013), but a potential connection between this variability and the dominant 2-year period of variability of the Madagascar phytoplankton bloom has not been examined. This dipole mode consists of anomalously higher SSTs over the western Indian Basin and lower SSTs off of Sumatra. At the same time, equatorial surface winds weaken and reverse direction from their usual east direction and precipitation increases over the western ocean basin and tropical eastern Africa. The connection between these fields involves the set-up of SST anomalies, which creates a change in the pressure field that induces the trade winds to converge downstream. This convergence enhances moisture supply that would cause increased precipitation and effectively cool SSTs in the western tropical region. Therefore, surface winds and SSTs are shown to be connected through the precipitation field.

The biennial tendency of this ocean-atmosphere system has been described theoretically Meehl (1993), which could be controlled by the upper ocean heat content in the Indian and Pacific oceans. This theoretical mechanism requires anomalously cool SSTs to persist for one year over a region with a season of local convective maximum, which would induce less evaporation, weak convection and weak winds, setting up warmer SSTs into the next year of the cycle. When the season of local maximum convection arrives again, the warmer SSTs would induce higher evaporation, stronger convection and stronger winds.

The mechanism behind this dipole mode could help explain the phytoplankton bloom, as weaker surface winds and cooler SSTs are seen in the Madagascar region during austral summer when blooms form. However Saji et al. (1999) focused on the region +/- 20° around the equator when describing the dipole mode and the bloom occurs further south. Therefore, evidence of the dipole mode in the Madagascar region is presented here. This evidence includes the presence of the dipole mode in eigenvectors of zonal winds, precipitation rates and PAR and correlation maps between these fields, along with the presence of an approximate 2-year period of variability in Chl concentrations, zonal winds, precipitation rates, SSTs, PAR, STR and MLD in the Madagascar region.

The dominant mode of variability in zonal winds includes both positive variability over the northern region and smaller negative variability over the southern Madagascar region, transitioning at approximately 18°S. This north-south dipole is also seen in the correlation map of this field with the PAR PC time series, with positive correlations north of Madagascar and negative correlations south of Madagascar and over Madagascar. PAR is largely affected by cloud cover, which would be associated with increased rainfall. Therefore, stronger winds are associated with lower PAR and more cloud cover and weaker surface zonal winds are associated with higher PAR and less cloud cover in the area of bloom formation. These associations are

opposite north of Madagascar where stronger winds are correlated with more PAR and less cloud cover. This is similar to the dipole mechanism outlined by Saji et al. (1999) where precipitation is enhanced where trade winds are strengthened and extended.

Dipoles are also seen in the dominant modes of variability in precipitation rates and PAR over the Madagascar region, with the transition occurring over Madagascar. The dipole in these fields exists between the northeast and southwest regions, with positive variability in the northwest and negative variability southeast in both fields. This same northeast-southwest dipole is seen in the correlation map of precipitation rates with PAR, with large positive correlations in the northeast and large negative correlations southwest. This map indicates that higher precipitation rates are correlated with lower PAR southwest of Madagascar and higher PAR northeast of Madagascar. PAR and precipitation rates are usually tightly correlated because increased precipitation rates are associated with cloud cover that lowers insolation reaching the surface ocean, which is represented in the southwest region of the correlation map. The positive correlations between these fields northeast of Madagascar represents the idea that when precipitation rates are higher over the southwest region they are low over the northeast region and this mechanism is correlated with PAR.

A dipole mode is not shown in the first mode eigenvector of SSTs from PCA, but it is seen in the composite map of SST anomalies in March. In March, warmer SSTs are seen south of Madagascar and negative anomalies occur north of Madagascar, transitioning around 20°S. This dipole persists through August (not shown) before it begins to exhibit positive anomalies over the full Madagascar region. The PC time series of SSTs is slightly positively correlated with zonal winds (R= 0.11) where cooler SSTs are correlated with weaker winds, but are not correlated with precipitation rates. Zonal winds are correlated with precipitation rates (R= -0.27), where increased rates would occur with weaker winds.

Precipitation rates are also correlated with lower PAR and higher STR, yielding large correlation values of -0.74 and 0.59, respectively. These fields are tightly correlated because a higher precipitation rate would indicate more cloud cover, which would cause less PAR to reach the surface ocean, and STR can be used as a proxy for precipitation rate (Saji et al., 1999). PAR is correlated with zonal winds (R= 0.21) but not with SSTs and STR is correlated with SSTs (R= 0.16) but not with zonal winds. Therefore, an increase in zonal winds is correlated with increased PAR and less cloud cover and higher surface thermal fluxes are correlated with warmer SSTs.

The biennial tendency of this dipole mode in the ocean-atmosphere system is supported here by presence of an approximate 2-year period of variability in many of the fields examined. The biennial tendency of this ocean-atmosphere system has been identified and described theoretically (Meehl, 1993; Saji et al., 1999), connecting the upper ocean heat content with atmospheric moisture content and wind variability on a 2-year timescale (Meehl, 1993). Zonal wind around the equator (+/-10°) in the Indian Ocean is known to exhibit a biennial tendency, with the winds oscillating between the Monsoon system and the Wyrtki-Meyers Pacific trade wind fields. The zonal wind field is reportedly made up of an equatorially trapped wave moving from the Indian to Pacific ocean and a standing wave that is made up of a node over Indonesia and maxima in the Indian and western Pacific oceans (Barnett, 1983). Variability in zonal winds includes a 24-month period of variability, indicating that the biennial tendency extends to the Madagascar region. An exact 24-month (2-year) signal is also seen in Chl concentrations and MLD, and a slightly longer period of approximately 28-months is seen in precipitation rates, SSTs, PAR and STR.

The biennial tendency of the phytoplankton bloom is evident, with blooms occurring almost every other year. In connecting the bloom to the dipole mode, precipitation rates and SSTs are significantly correlated with Chl concentrations, but zonal winds are not. Precipitation rates over the greater Madagascar region are negatively correlated with Chl at both 2-month (R= -0.29) and 1-month (R= -0.26) lags. Additionally, SSTs are correlated with Chl concentrations when SSTs lag Chl concentrations by 2 months (R= 0.17). These correlations support the idea that lower precipitation rates precede higher Chl concentrations, which precede higher SSTs.

4.4. Dipole mode versus El Niño-Southern Oscillation

Equatorial winds are tightly correlated (R= |0.6|) with the dipole mode in SSTs, represented by the Dipole Mode Index (DMI). DMI is constructed from anomalies in the SST gradient between the western (50°-70°E, 10°S-10°N) and south eastern tropical Indian Ocean (90°E-110°E, 10°S-0°N), where a positive dipole event involves cooler than normal SSTs are found in the eastern region and warmer than normal SSTs are found in the western region. It was previously thought that DMI was a product of ENSO and not an independent process, but they do not always coincide (Saji et al., 1999; Saji & Yamagata, 2003; Meyers et al., 2007), with a correlation of <0.35.

Chl correlations with the indices shows a positive correlation with DMI (R= 0.21) and a negative correlation with Niño3.4 (R= -0.23). These correlations occur at different lags where DMI lags Chl by 6 months and Chl and the Niño index are correlated at zero lag. Furthermore, bloom years usually coincide with negative Niño events and non-bloom years occur with the largest positive Niño events (Figure 21). Interesting correlations are also seen in the zonal wind and SST fields. Zonal wind correlations are negative with both indices, but the lags in the correlations span over a year, where decreased winds lag DMI by 5 months (R= -0.12) and Niño lags behind winds by 7 months (R= -0.11). SSTs have a much higher correlation with the Niño3.4 index (R= 0.36 versus R= 0.12), indicating that SSTs are much more influenced by Niño than the dipole mode. Precipitation rates, STR, PAR and MLD also showed significant correlations with both indices, but the correlations were approximately equal in magnitude with each index. DMI and Niño3.4 indices have a correlation of R= 0.24, which is lower than what Saji et al. (1999) found, but still does not rule out the possibility of DMI being an extension of ENSO. Therefore, the influence of mechanisms represented by the DMI and Niño indices on the fields listed above requires further analysis.

4.5 Conceptual Diagram

With the lack of evidence supporting either of the existing hypotheses regarding the Madagascar phytoplankton bloom, we introduce an alternate explanation based on the biennial tendency of the dipole mode in the ocean-atmosphere system. This hypothesis requires that anomalously cool SSTs and weaker winds set up over the bloom region. These anomalies induce lower surface thermal radiation fluxes, followed by lower precipitation rates and increased PAR. Anomalously high PAR favors phytoplankton growth in the region south of Madagascar.

This hypothesis is supported by results from both PC correlations and composite maps. Increased Chl concentrations are correlated with lower precipitation rates, lower STR fluxes and higher PAR, with maximum correlations when increased Chl occurs two months after changes in these other fields. Additionally, precipitation rates, STR and PAR all show high correlations with

each other with zero lag between fields. Both precipitation rates and PAR are correlated with zonal winds and STR and MLD are correlated with SSTs with zero lag. Finally, Chl and SST fields are correlated when Chl concentrations precede SSTs by 2 months.

At a 2-month lag, increased Chl following, Chl is negatively correlated with precipitation rates over the greater region and STR and positively correlated with PAR based on the dominant mode of variability in Chl data. At a 1-month lag, Chl is again negatively correlated with precipitation rates over the greater region and STR and positively correlated with PAR but at lower correlation values. Additionally, Chl is negatively correlated with precipitation rates over Madagascar at a 1-month lag. At zero lag, Chl is not significantly correlated with any of these variables, however many of the oceanic and atmospheric variables are correlated with zero lag. Zonal winds are correlated with precipitation rates over both the greater region and over Madagascar, PAR and SSTs. Precipitation rates over the greater Madagascar region are correlated with PAR and precipitation rates over Madagascar and precipitation rates over Madagascar are also correlated with PAR. Finally, SSTs are positively correlated with Chl at a 2-month lag, Chl preceding. SSTs are also positively correlated with MLD, which is not correlated with any other parameter at a 0-month lag.

However, MLD is correlated with precipitation rates (R= -0.24) and STR (R= -0.22) at a 6-month lag and Chl (R= 0.24) at a 4-month lag when MLD follows. Approximate 6-month lagged correlations are also seen between SSTs and other fields, including Chl, STR and PAR. SSTs are correlated with Chl concentrations (R= -0.19) and zonal winds (R= -0.19) at an 8-month lag, SST following, indicating that the development of a phytoplankton bloom and increased zonal winds would be followed by cooler SSTs 8 months later. Cooler SSTs also follow increased STR fluxes (R= 0.17) and lower PAR (R= -0.16) at a 5-month lag. Composite maps of bloom years show that SSTs are anomalously low before the bloom and then become anomalously high in March, after blooms have formed. Expanding on the composites for the full year between bloom and non-bloom years (not shown) shows that SSTs are anomalously low over the bloom region leading up to the bloom initiation from September to February and then becomes positive and remains positive from March to August, representing an approximate 6-month cycle.

This ocean-atmosphere biennial mechanism hypothesis is also supported by results from composite maps of the differences between bloom and non-bloom years. Examining composite maps for all months of the year for the other fields (not shown), the largest anomalies occur during austral summer for all fields except MLD, which are largest in austral winter. SSTs are anomalously low and zonal winds are anomalously weak from December to February, with lowest wind anomalies in February. By March, SSTs have become anomalously warmer. Anomalies in surface thermal fluxes, precipitation rates and PAR are largest in December compared to all months. However, these anomalies are the opposite of what is expected for bloom formation, including higher thermal fluxes, higher precipitation rates and lower PAR. Moving into January, anomalies in these fields switch, showing lower thermal fluxes, lower precipitation rates and higher PAR. These anomalies persist in February east of Madagascar where the bloom usually propagates before dying out. The December to January transition in these fields could indicate a pre-conditioning of the ocean-atmosphere system before the bloom begins that encourages a signal reversal, but this requires further analysis. Lastly, surface currents south of Madagascar show stronger eastward-flowing and weaker westward-flowing currents, which control the propagation of the bloom away from Madagascar.

Anomalies in MLD show a deeper mixed layer south of Madagascar in December and shallower mixed layer depths in January that again becomes deeper in February. However, these anomalies are small compared to differences 6 months later in austral winter. Larger anomalies between bloom years and non-bloom years during this time period explain the correlations seen between the PC time series of the dominant mode of variability in this field with STR, precipitation rates and Chl. From composite maps of MLD, large anomalies south of Madagascar are seen in August, which would be approximately 6 months before typical bloom initiation.

The anomalies between bloom and non-bloom years and the approximate 2-year period of variability in oceanic and atmospheric variables suggest that a biennial tendency is present in this region. This biennial tendency has already been identified in the greater tropical Indian Ocean region (Saji et al., 1999), but had not been linked to bloom formation. The conceptual diagram relating these fields connects anomalously cooler SSTs and weaker winds to decreased surface thermal fluxes to reduced precipitation and cloud cover to higher PAR and increased phytoplankton growth. This conceptual framework supports a connection between the winds and SSTs through the precipitation field, where warmer SSTs and weaker winds precede lower precipitation rates, which precede the warmer SSTs that develop in March. The framework also supports the biennial mechanism outlined by Meehl where cooler SSTS, lower STR and weaker winds occur in bloom years, which are followed by warmer SSTs, higher STR and stronger winds in the non-bloom year. However, SST anomalies do not appear to persist for an entire year, which is a pre-condition to Meehl's theory.

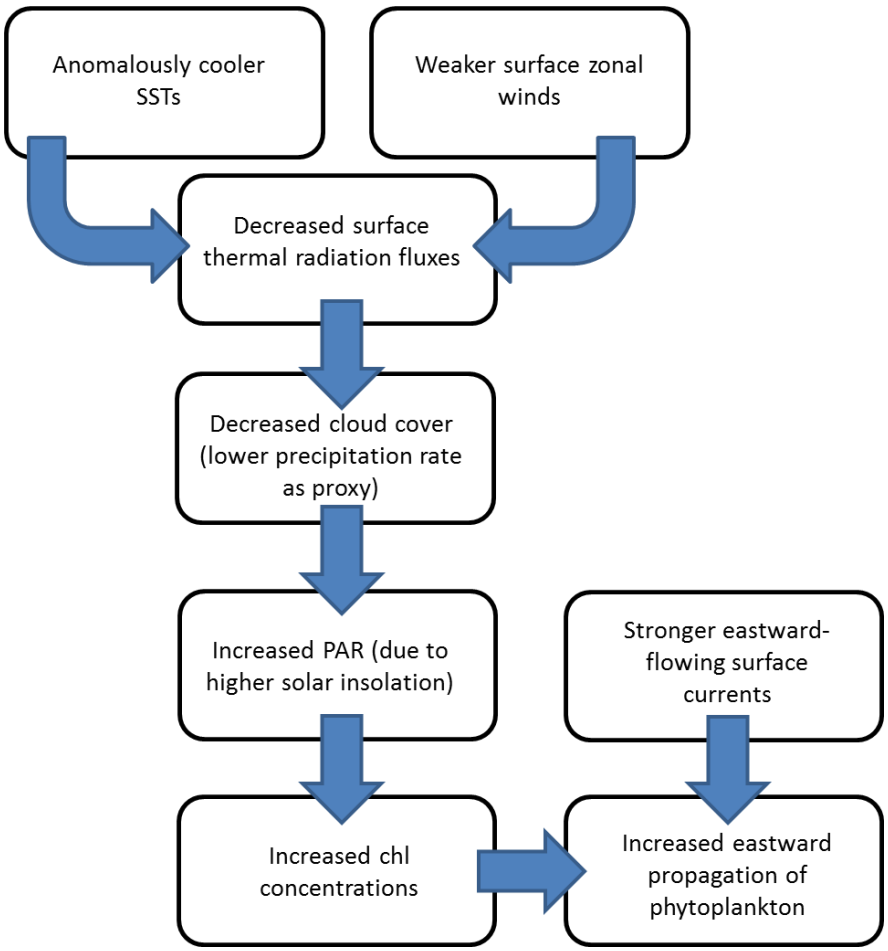

5. Conclusion

Neither of the existing hypotheses of mixed layer depth and iron fertilization was supported by this research to explain bloom initiation southeast of Madagascar. Instead, an alternative hypothesis is presented here involving the existence of a biennial ocean-atmosphere mechanism in the Indian Ocean controlled by the upper ocean heat content and zonal winds in connection to bloom. This mechanism is represented by anomalies in SSTs, zonal winds, precipitation rates, PAR, STR and, lastly, Chl concentrations that act on a dominant biennial timescale.

The mixed layer depth hypothesis is discounted by the presence of shallower mixed layer depths, Chl correlations with higher SSTs and weaker winds during the time of bloom formation. Composite maps of MLD showed a shoaling of mixed layer depth in January through March when most blooms form. Also, higher Chl concentrations are correlated with higher SSTs based on their PC time series at a 2-month lag. Finally, zonal winds are weaker in January through March over the area of bloom formation, discrediting the existence of stronger southeast trade winds with blooms. It is important to note that anomalies in zonal winds and MLD are higher in December before bloom formation and SSTs are warmer in March, after most blooms have formed, but the timing of these anomalies and their correlations with Chl do not support an influence on bloom initiation. Furthermore, composite maps of SSTs do show cooler SSTs from December to February in bloom years compared to non-bloom years but this association alone does not allow definitive support of the mixed layer depth hypothesis.

The alternative iron fertilization hypothesis was also not supported by this analysis. While we did find a correlation between the first mode PC time series of Chl concentrations over the bloom region and precipitation rates over Madagascar, the correlation was negative, indicating that increased Chl is associated with lower precipitation rates instead of the higher rates characteristic of a cyclone. We were also able to examine the new sea surface salinity data from NASA's Aquarius, which should show lower SSS in the region of bloom propagation if runoff is prominent in the region. Instead, we found approximately similar values in both bloom and non-bloom years with marginally lower values in the non-bloom years. Furthermore, the evolution of this data supports a remote source of lower-salinity waters coming from the SEC. However, the Aquarius mission only began in 2011 so we were only able to analyze data from 2012 to 2014, not allowing for a robust assessment. The correlation between the number of cyclone landings and increased Chl concentrations found by Uz (2007) also remains unclear. It could be that the mechanism controlling precipitation rates over the bloom region and over Madagascar also controls bloom formation, creating correlation without causation. Surface ocean currents do support circulation of water away from the island into the region of bloom propagation southeast of Madagascar but the lack of supporting evidence in precipitation and SSS data requires lead us to reject the iron fertilization hypothesis.

Due to the lack of evidence supporting either hypothesis, we propose an additional hypothesis involving an ocean-atmospheric biennial mechanism as the cause of bloom initiation in the Madagascar region. A biennial mechanism in the tropical Indian Ocean has been identified but had not been examined for connection to the bloom. This mechanism is caused by variability in the upper ocean heat content and its influence on winds and evaporation in the region. The anomalies in SSTs in the greater Madagascar region indicate that SSTs are cooler going into austral summer, along with weaker winds, which are followed by lower evaporation (STR fluxes as a proxy). The lower cloud cover associated with less evaporation allows a larger amount of

PAR to reach the surface waters and encourage phytoplankton growth. The increase in eastward flow in surface currents encourages the propagation of the bloom, and the phytoplankton follow the movement of the eddy field including both cyclonic and anti-cyclonic eddies.

In conclusion, the potential influence of an ocean-atmosphere interaction in the Indian Ocean on bloom formation is evident. Principle component analysis on both oceanic and atmospheric variables in the greater Madagascar region shows the presence of a 2-year period of variability. Additionally, composite maps show the anomalies in evolution of these fields between bloom and non-bloom years leading up to bloom initiation. Results from both PCA and composite maps support the biennial mechanism hypothesis, and discredit both the mixed layer depth and iron fertilization hypotheses. This conceptual framework based on statistical relationships and dominant variability in the oceanic and atmospheric fields over Madagascar sets the foundation of an alternative hypothesis to bloom development and an improved understanding of the ocean-atmosphere interactions in this region. However, the connection to the bloom is still not resolved. We hypothesize that both irradiance and nutrient availability would influence phytoplankton growth but results from the mixed layer depth data to not resolve the source of nutrients. Nutrients could be sourced remotely or the MLD data we used could not be representative of the system. Additionally, the dominant periods present in the variability of these fields examined include an exact 2-year period, along with 28-month and 4-year periods. Resolving the specific influences of the biennial, Quasi-Biennial Oscillation (QBO), ENSO and DMI processes also requires further analysis.

This analysis focused on the interannual variability of bloom formation southeast of Madagascar, but variability is also shown in the spatial and temporal variations between blooms. Additionally, the initiation of the bloom initiation was focused on in this research, but the cause of the termination of the bloom is also up for debate. Also, this analysis allowed us to resolve dominant statistical patterns in individual datasets, but the ocean-atmosphere connections presented here could be improved with statistical analyses aimed to tease out n-dimensional relationships between oceanic and atmospheric variables and numerical modeling to improve the dynamical understanding of these relationships.

FIGURES

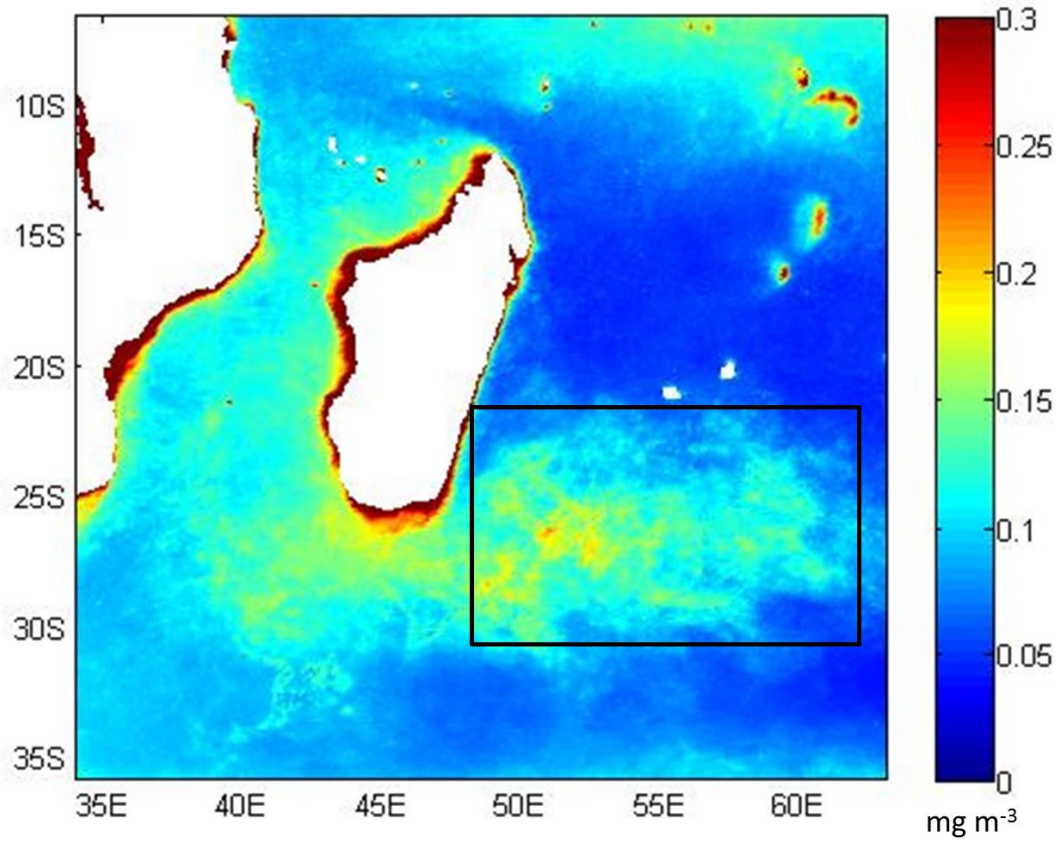

Figure 1. Spatially-averaged Chl concentrations (mg m^{-3}) from January-April of bloom years (1999, 2000, 2002, 2004, 2006, 2008, 2012). The area of highest concentrations is outlined in black (22-31°S, 49-62°E) and is defined as the most common bloom region.

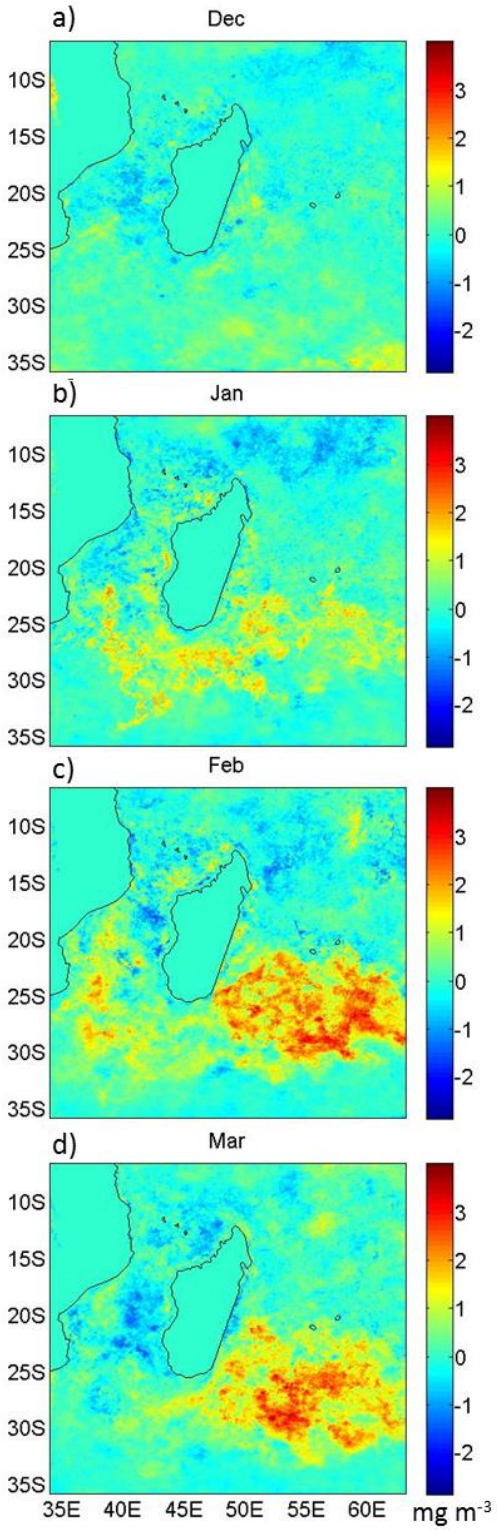

Figure 2. Composite maps constructed for a) December, b) January, c) February and d) March of the differences in Chl concentration anomalies (mg m^{-3}) between bloom (1999, 2000, 2002, 2004, 2006, 2008, 2012) and non-bloom years (1998, 2001, 2003, 2005, 2007, 2009, 2010, 2011).

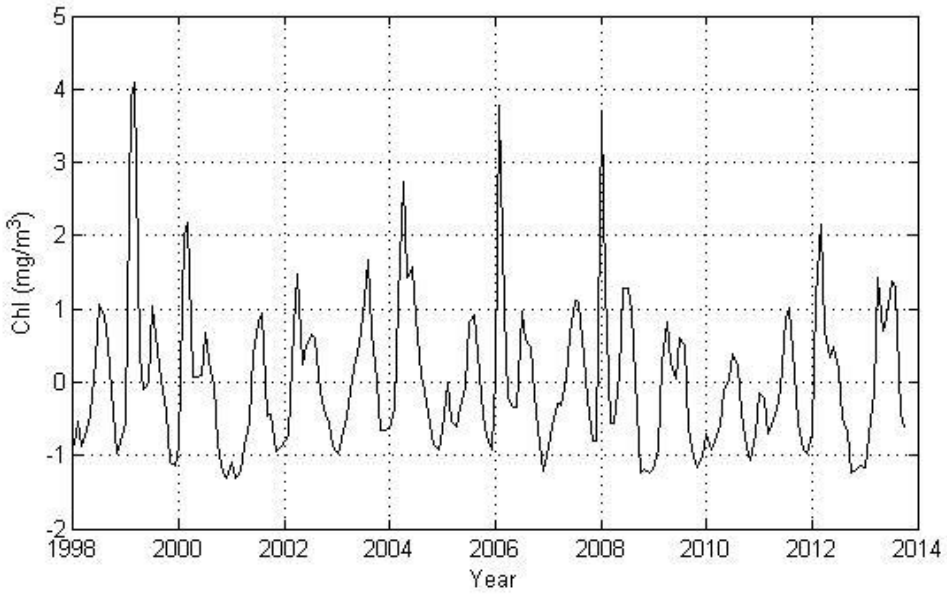

Figure 3. Normalized time series of Chl concentrations spatially-averaged over the most common area of bloom formation southeast of Madagascar (22-31°S, 49-62°E). The largest peaks indicate bloom years.

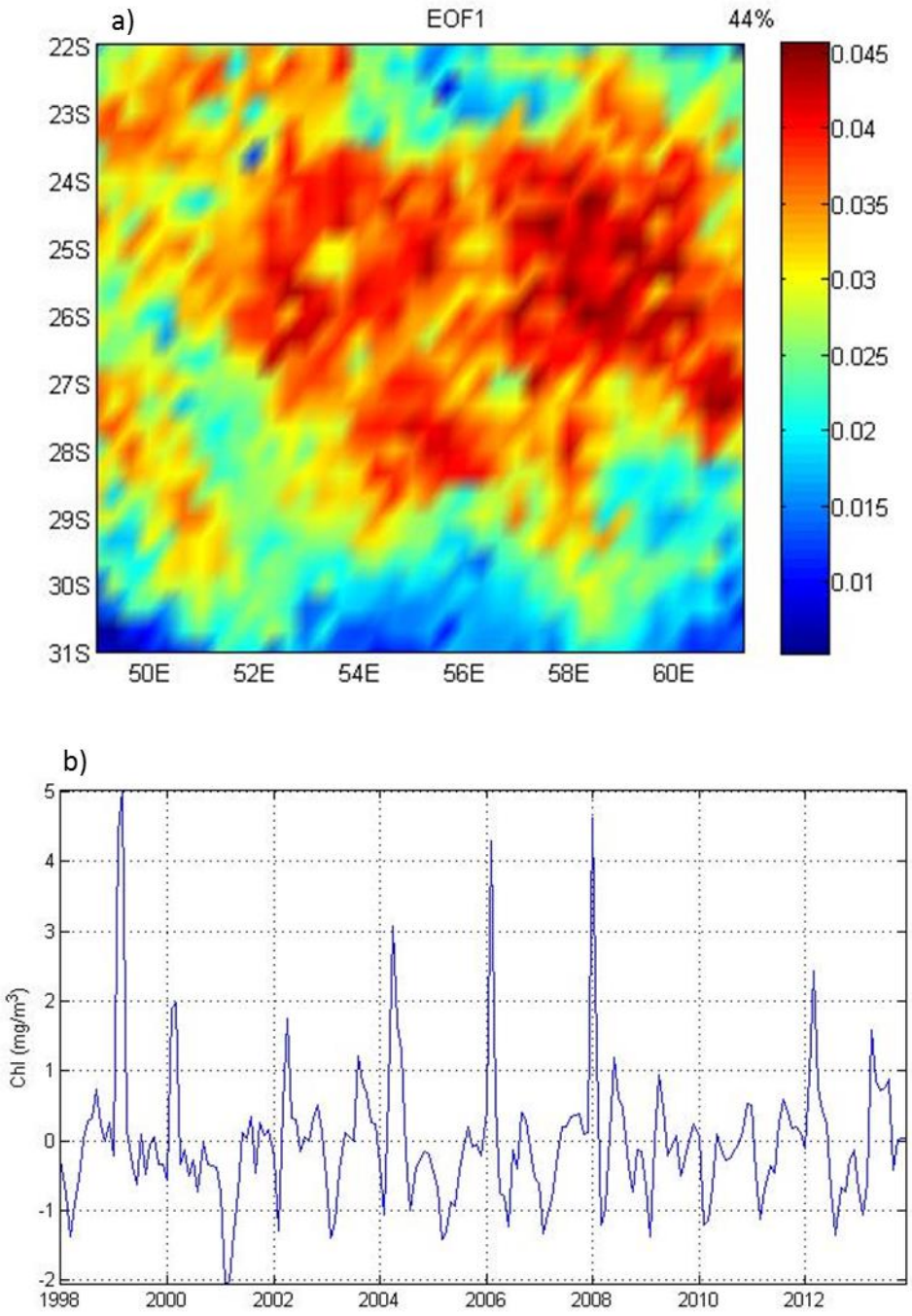

Figure 4. The first mode a) eigenvector and b) normalized principal component time series in Chl concentration data over the bloom region from principal component analysis, representing 44% of the variability in the data.

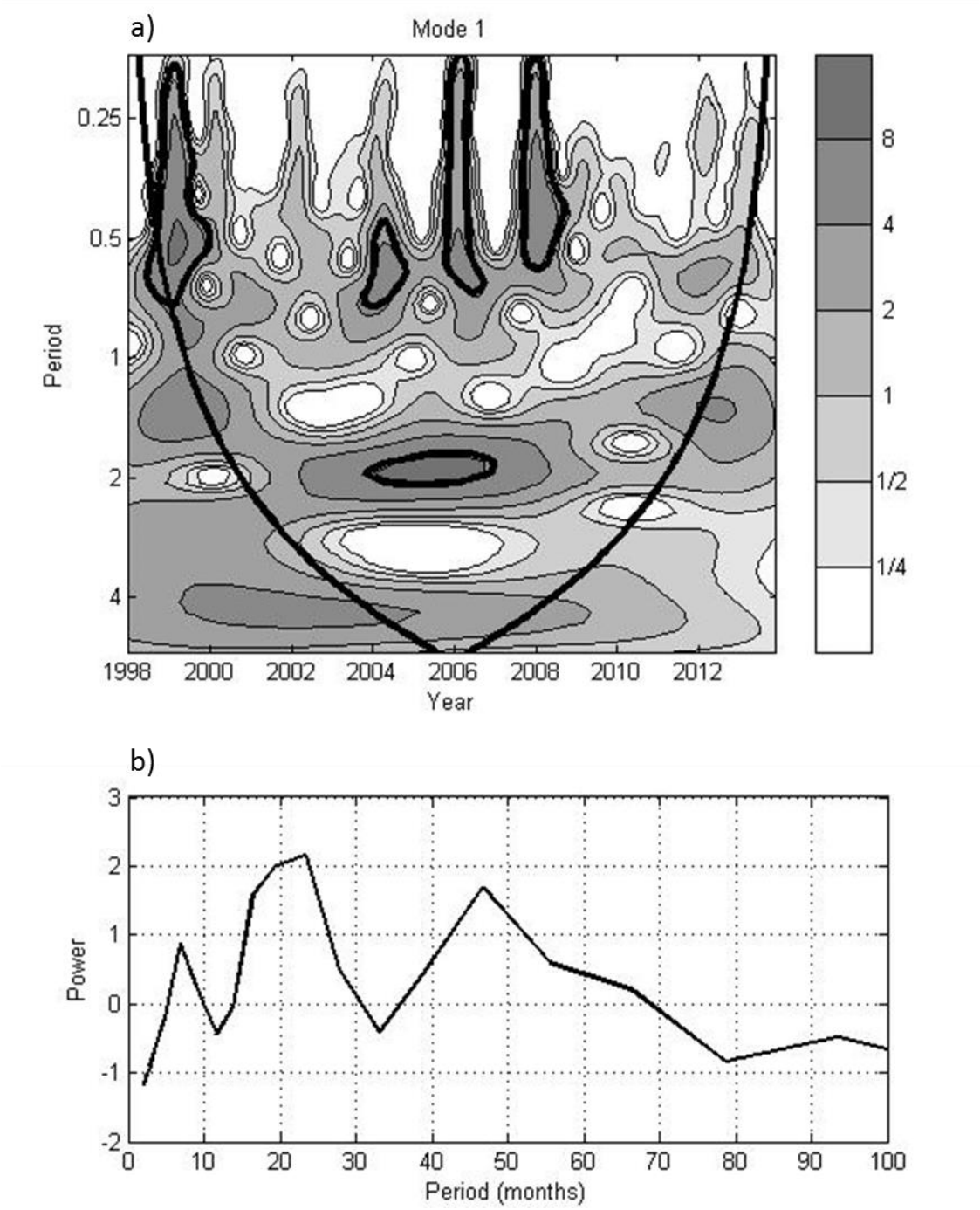

Figure 5. a) Time-period plot of the dominant mode of variability from PCA, where color bar represents the power at each time-period point and b) the power sum from the wavelet showing overall dominant periods.

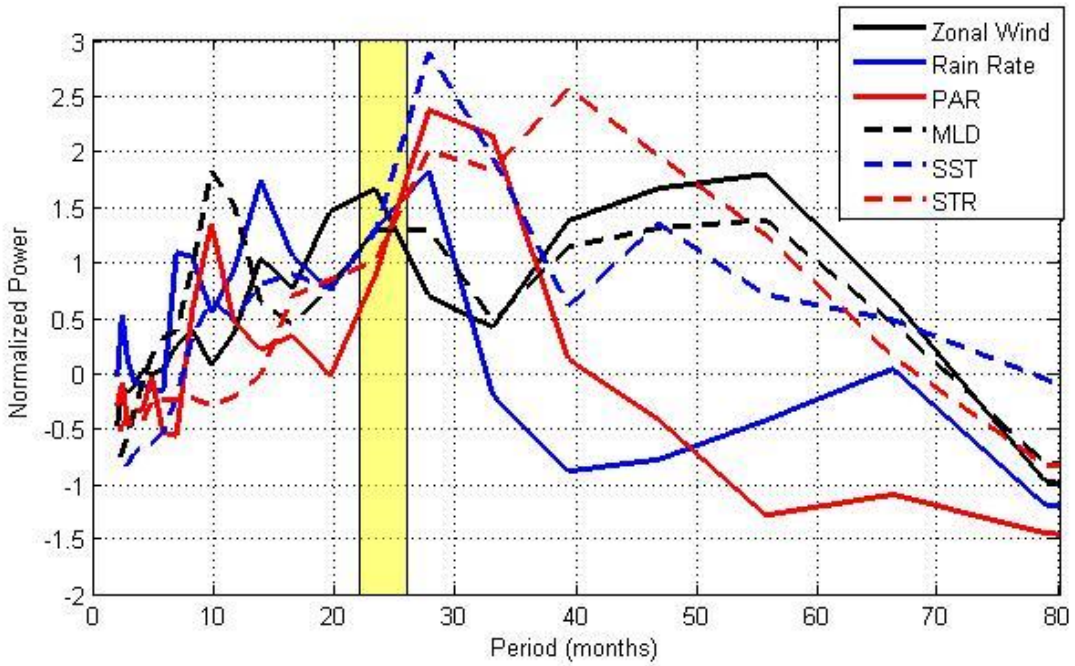

Figure 6. Power sums from the first mode principal component time series of zonal winds, precipitation rates, photosynthetically active radiation (PAR), mixed layer depth (MLD), SSTs and surface thermal radiation over the Madagascar region. The yellow bar represents the time period 22-26 months for comparison. Data were lopassed with a recursive Butterworth filter cut off at 70 months and power sums were normalized.

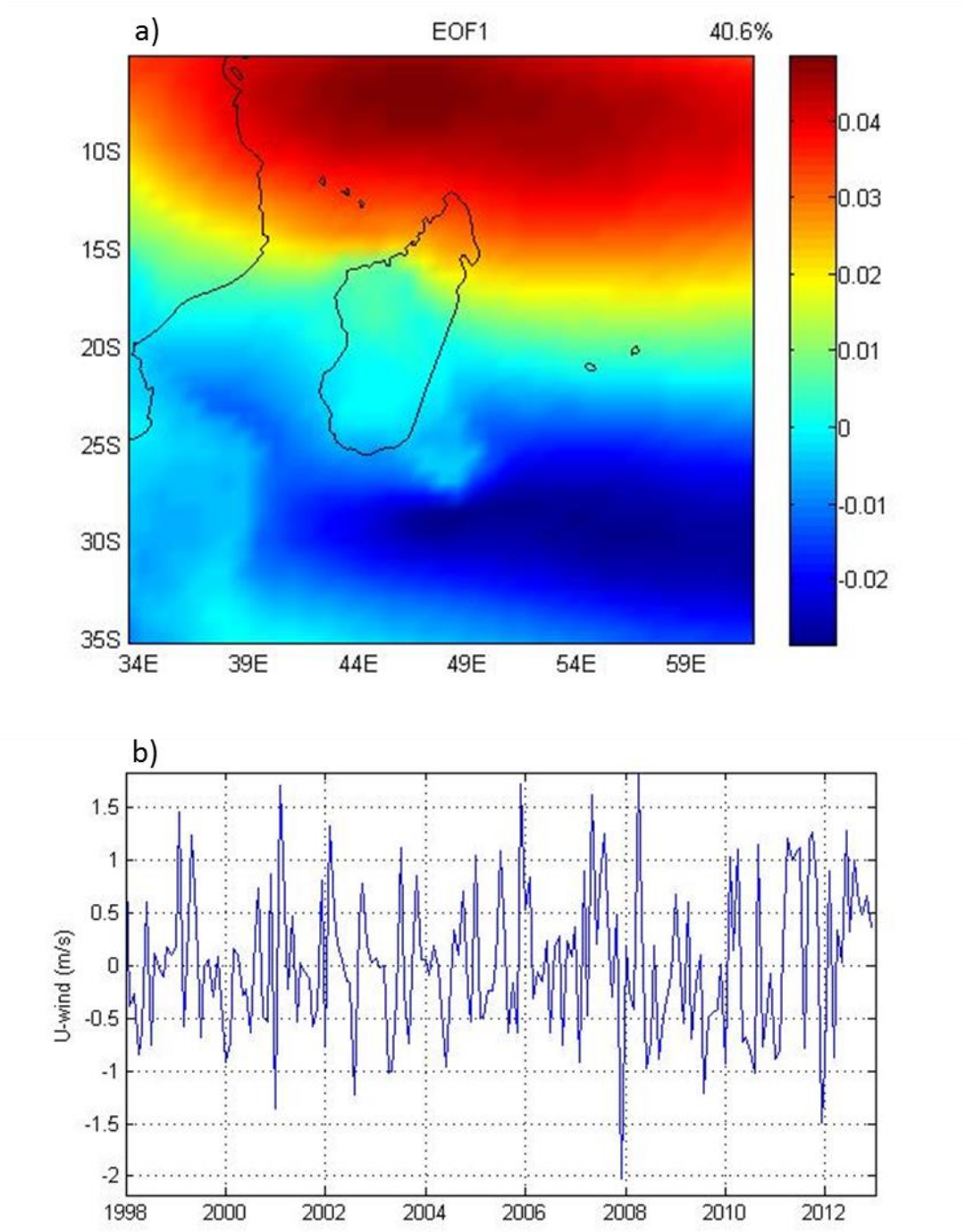

Figure 7. The first mode a) eigenvector and b) normalized principal component in zonal wind data over the Madagascar region from principal component analysis, representing 40.6% of the variability in the data.

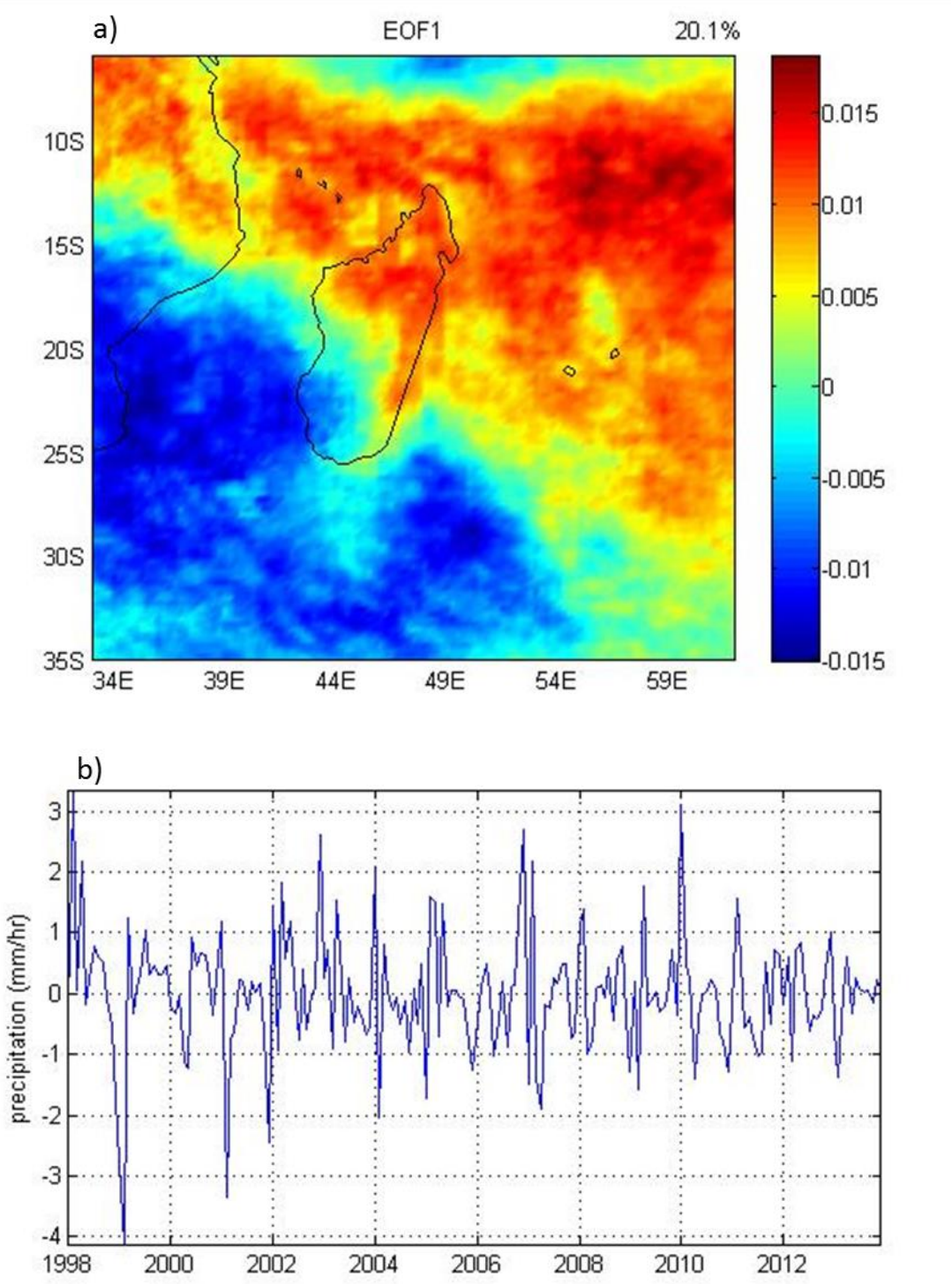

Figure 8. The first mode a) eigenvector and b) normalized principal component in precipitation rate data over the Madagascar region from principal component analysis, representing 20.1% of the variability in the data.

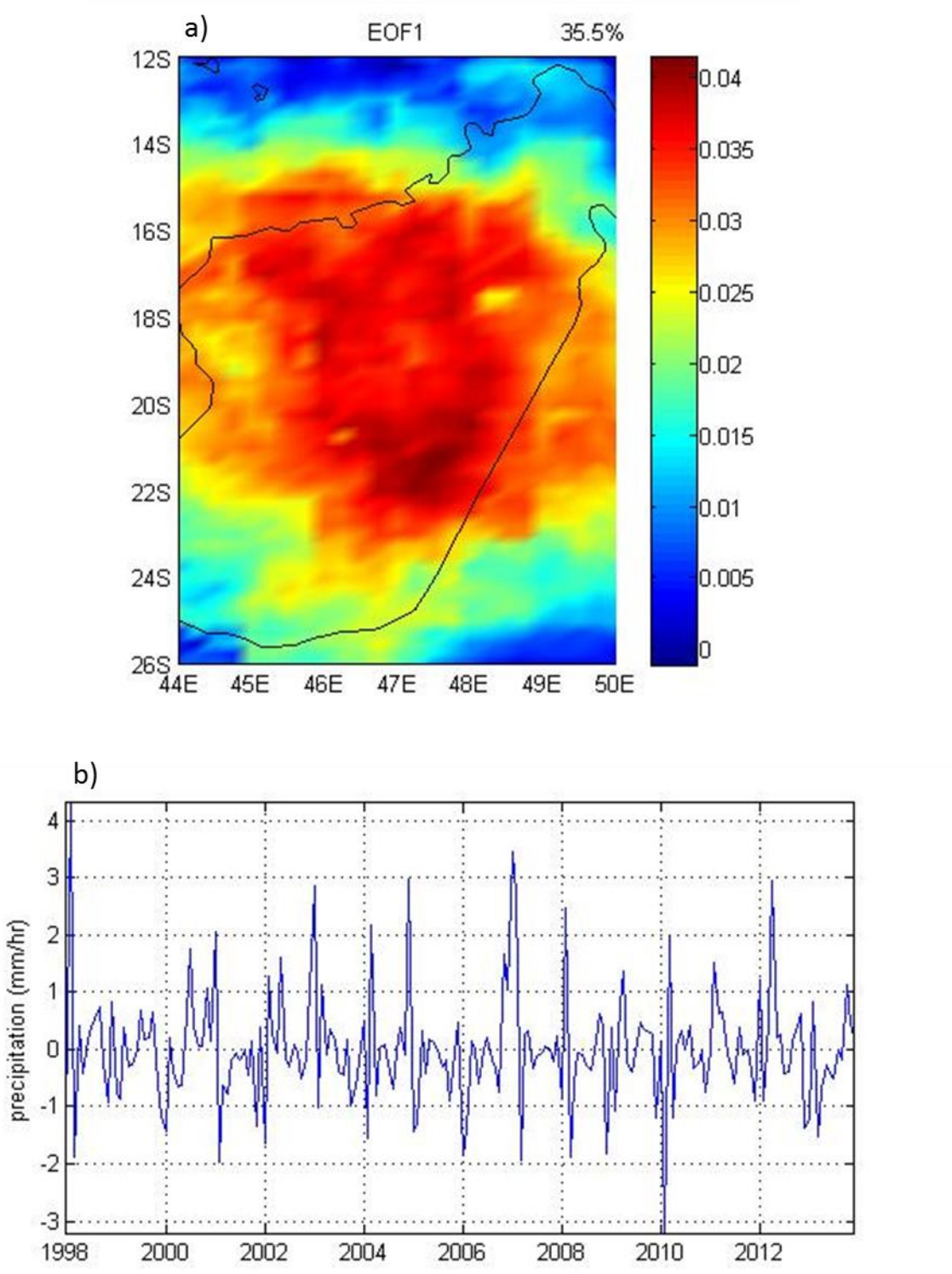

Figure 9. The first mode a) eigenvector and b) normalized principal component in precipitation rate data over Madagascar from principal component analysis, representing 35.5% of the variability in the data.

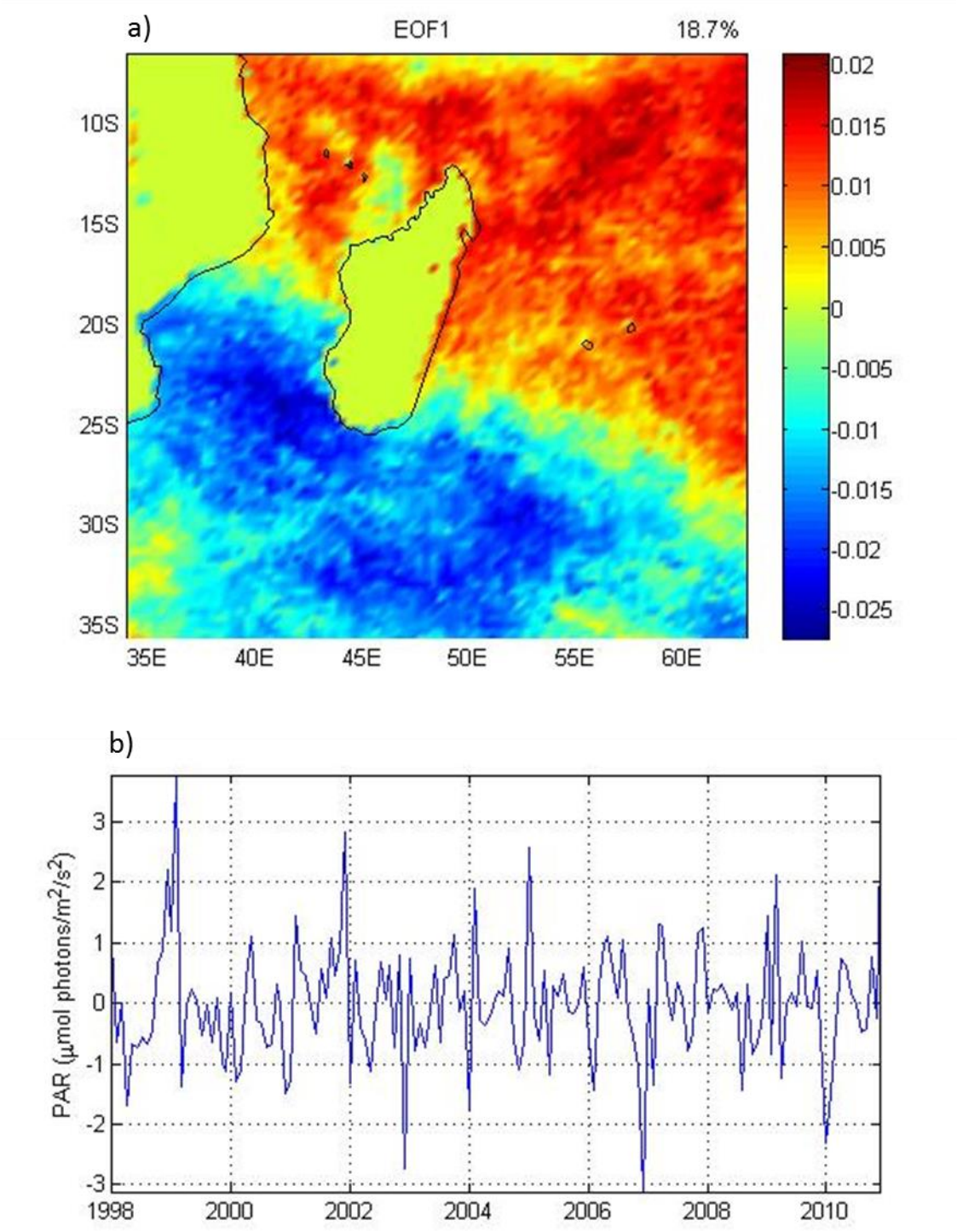

Figure 10. The first mode a) eigenvector and b) normalized principal component in photosynthetically active radiation data over the Madagascar region from principal component analysis, representing 18.7% of the variability in the data.

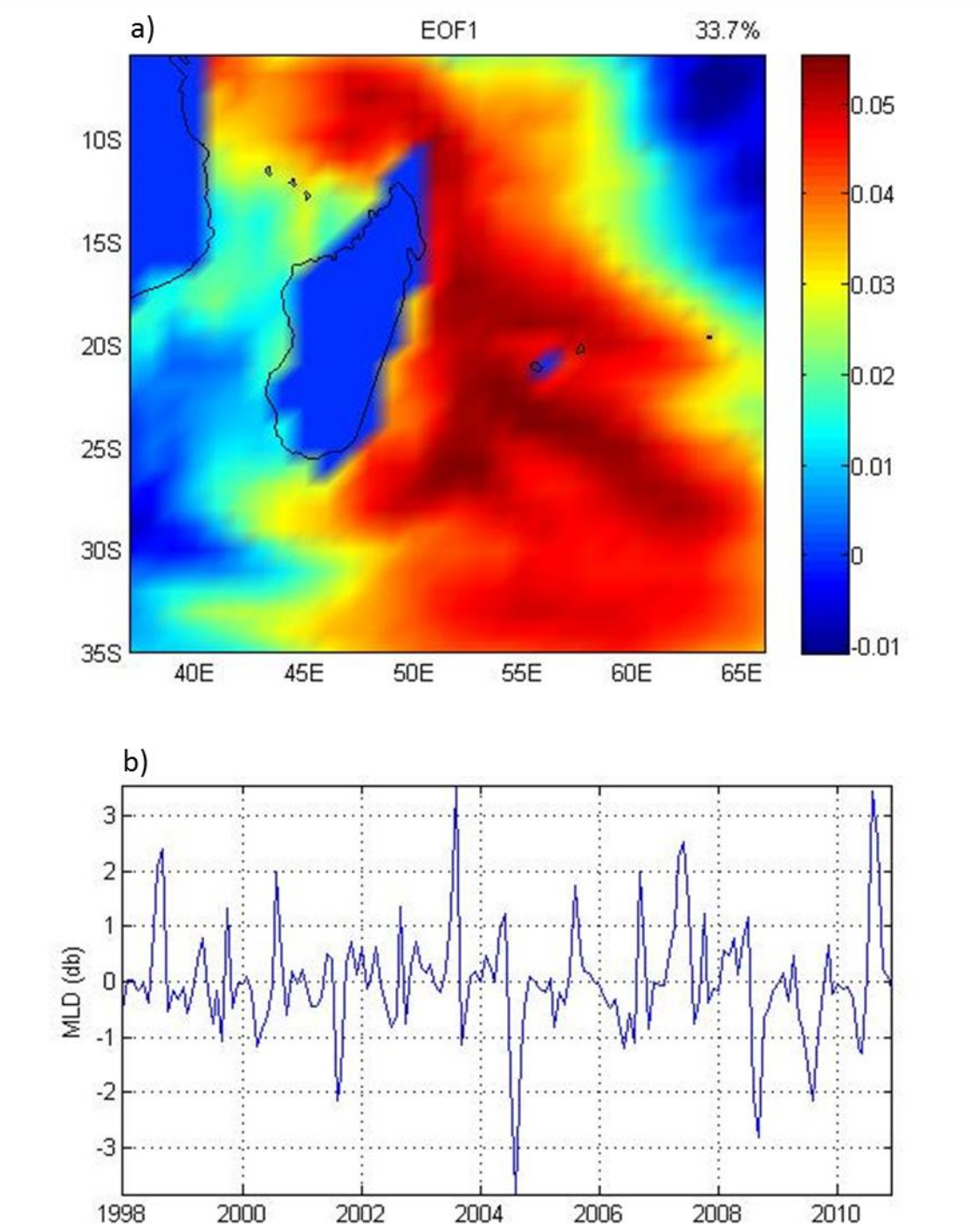

Figure 11. The first mode a) eigenvector and b) normalized principal component in mixed layer depth data over the Madagascar region from principal component analysis, representing 33.7% of the variability in the data.

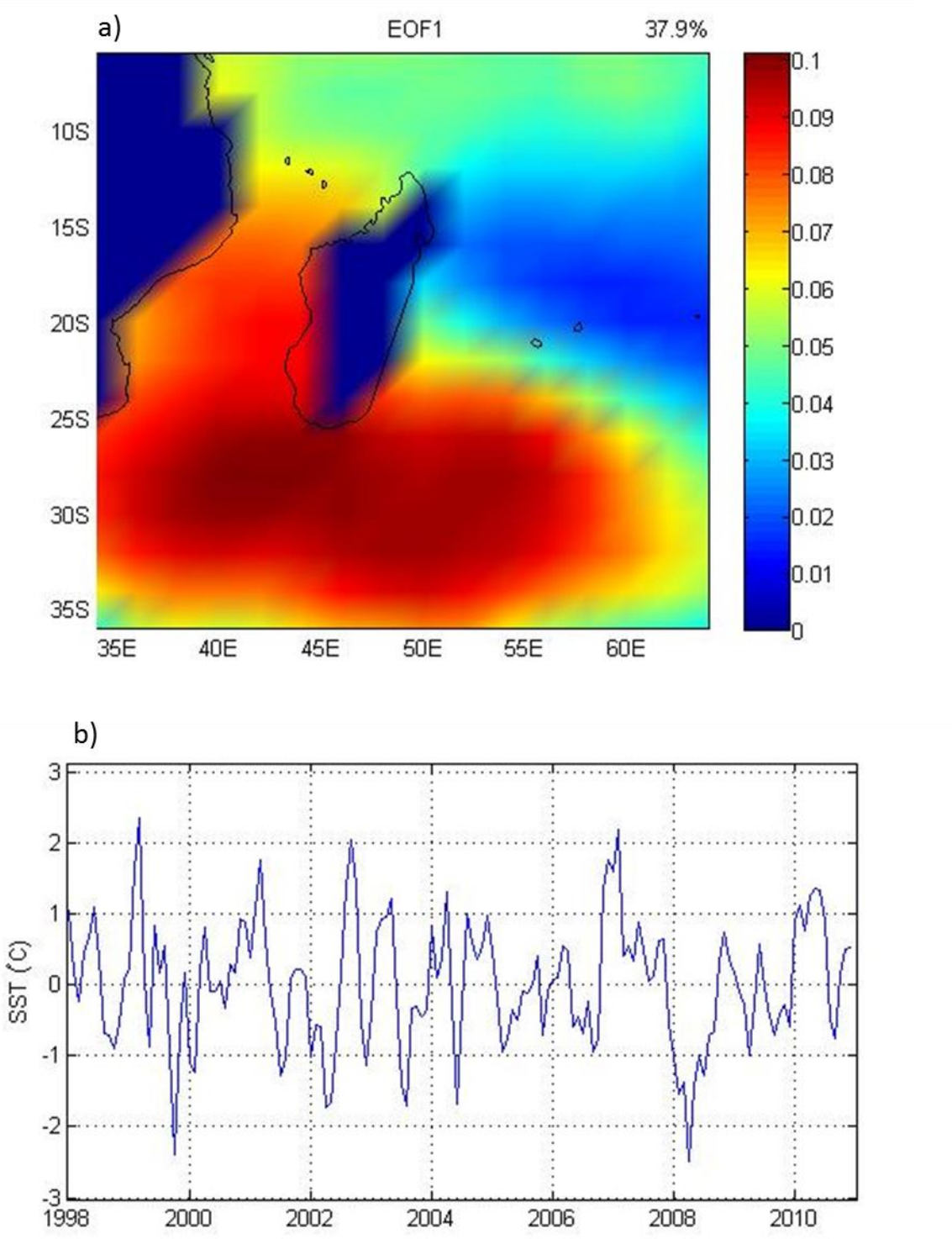

Figure 12. The first mode a) eigenvector and b) normalized principal component in sea surface temperature data over the Madagascar region from principal component analysis, representing 37.9% of the variability in the data.

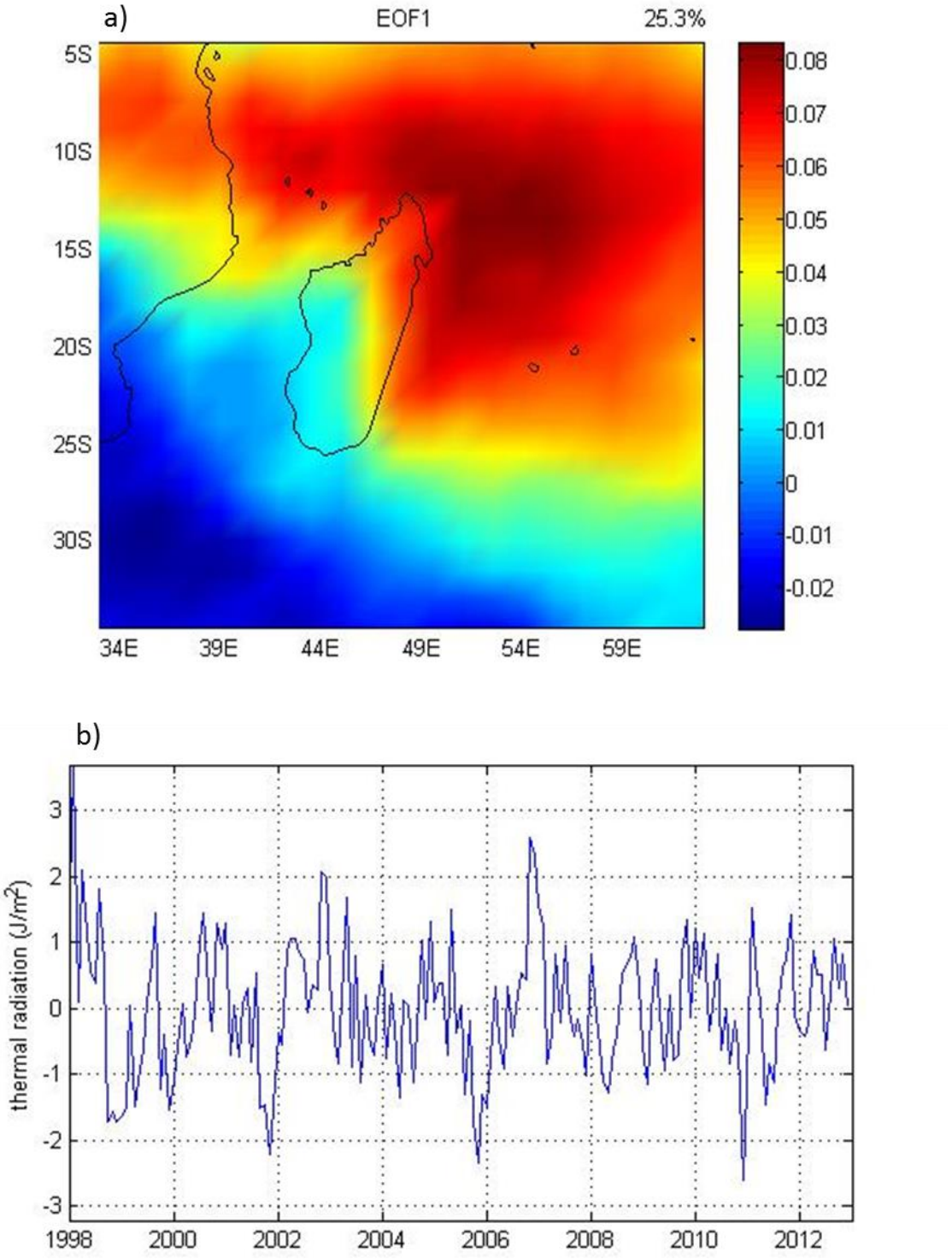

Figure 13. The first mode a) eigenvector and b) normalized principal component in surface thermal radiation data over the Madagascar region from principal component analysis, representing 25.3% of the variability in the data.

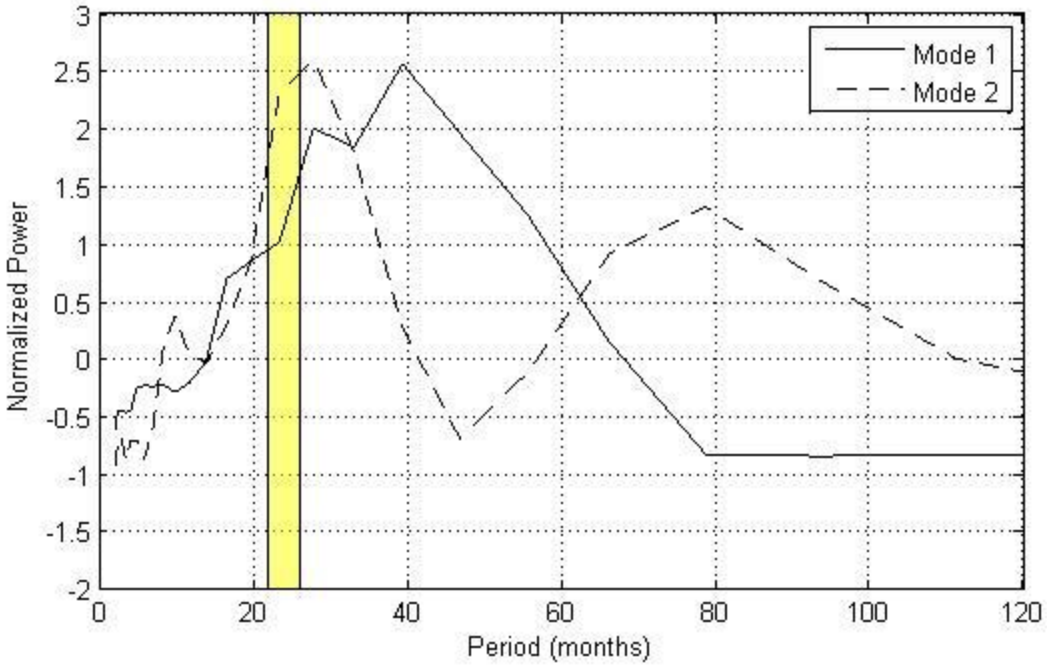

Figure 14. Power spectrums of the first and second modes of variability in surface thermal radiation data in the Madagascar region from PCA.

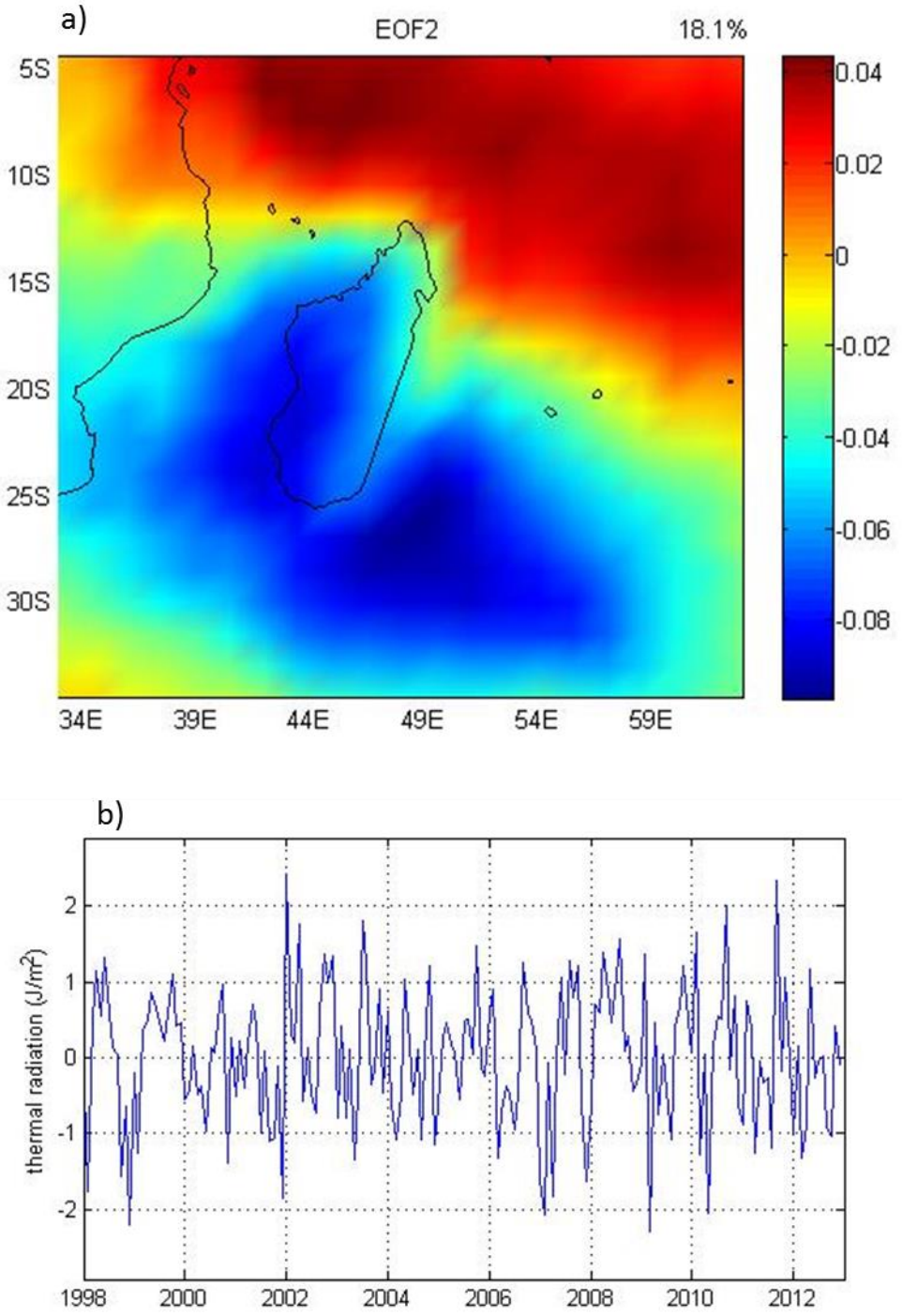

Figure 15. The second mode a) eigenvector and b) normalized principal component in surface thermal radiation data over the Madagascar region from principal component analysis, representing 18.1% of the variability in the data.

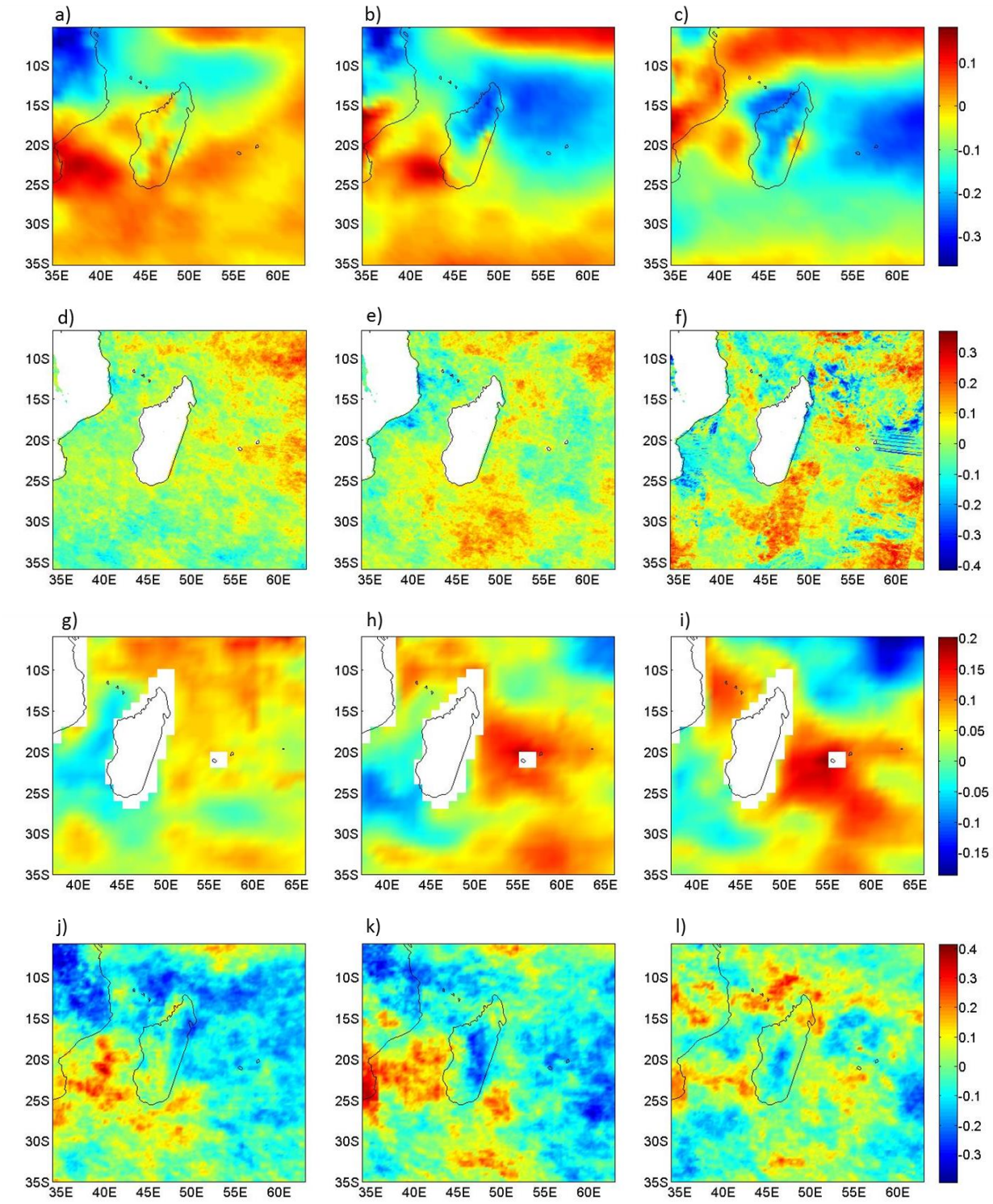

Figure 16. Correlation maps between the first mode PC time series in Chl data with normalized time series of a-c) zonal wind data, d-f) PAR data, g-i) MLD data and j-l) precipitation rate data at 2-month, 1-month and 0-month lags, respectively. Correlations with magnitude greater than +/-0.147 for zonal wind, +/-0.172 for PAR, +/-0.159 for MLD and +/-0.147 for precipitation rate were determined to be significant at the 95% confidence level.

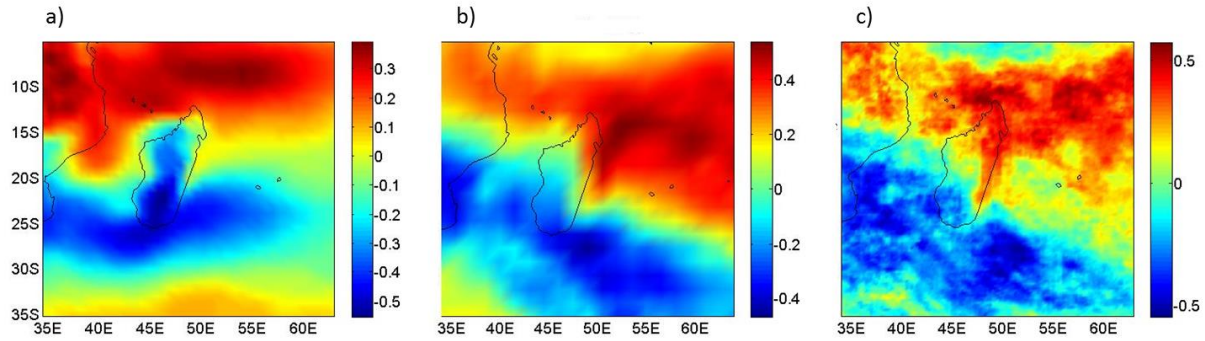

Figure 17. Correlation maps between the first mode PC time series of PAR with normalized time series of a) zonal wind, b) surface thermal radiation and c) precipitation rate data. Correlations with magnitude greater than +/- 0.16 were determined to be significant at the 95% confidence level.

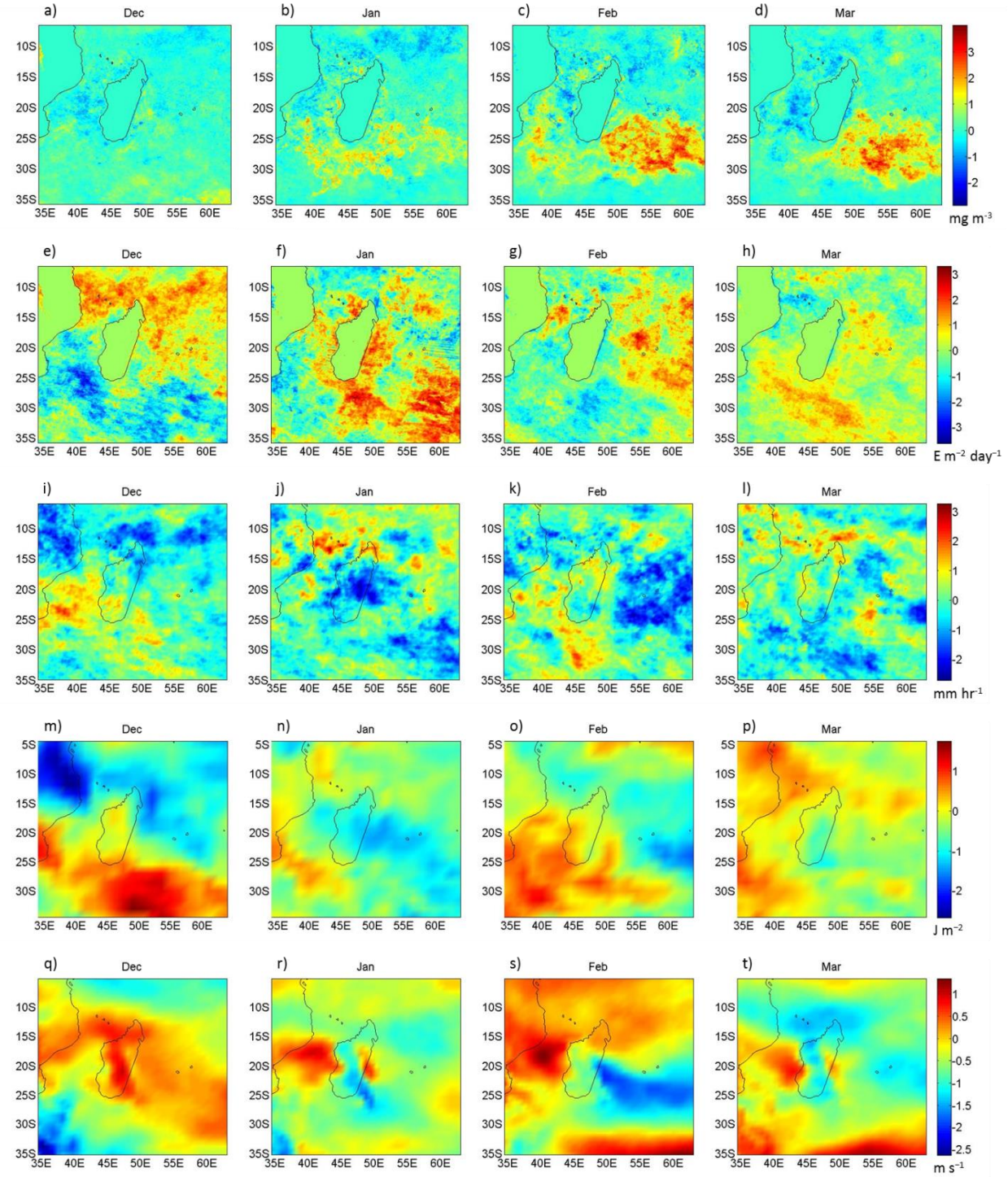

Figure 18. Composite maps constructed for December through March representing the difference in anomalies between bloom and non-bloom years for a-d) Chl concentrations, e-h) photosynthetically active radiation, i-l) precipitation rates, m-p) surface thermal radiation and q-t) zonal wind strength. Data has been normalized and climatology removed for all fields, then non-bloom anomalies are subtracted from bloom year anomalies.

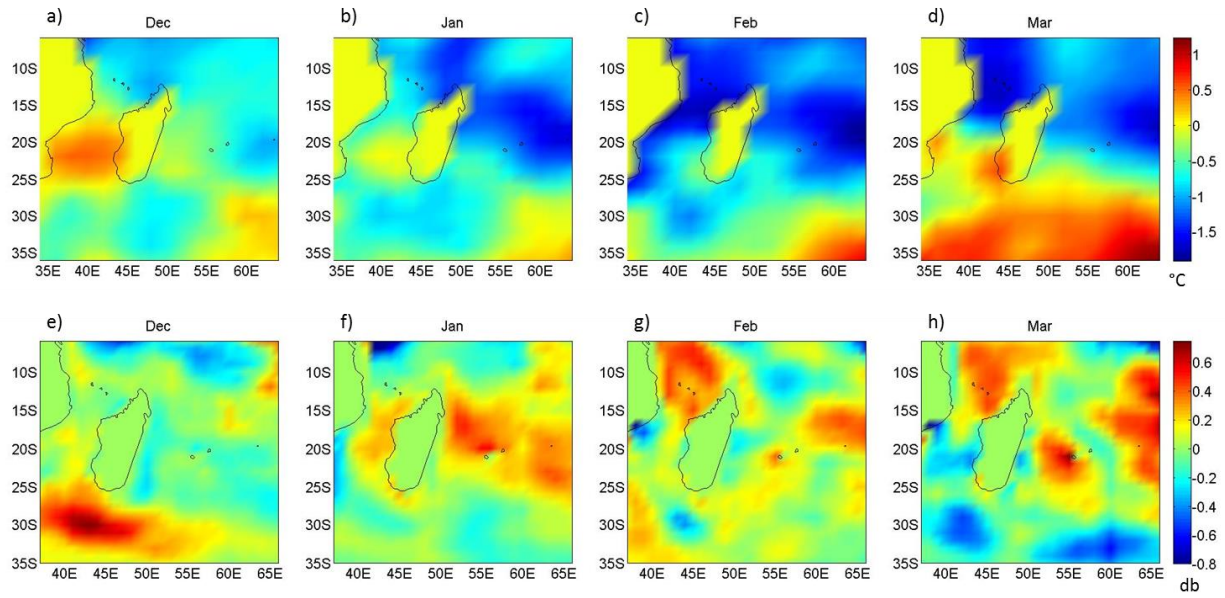

Figure 19. Additional composite maps constructed for December through March representing the difference in anomalies between bloom and non-bloom years for a-d) sea surface temperatures and e-h) mixed layer depths. Data has been normalized and climatology removed for all fields, then non-bloom anomalies are subtracted from bloom year anomalies.

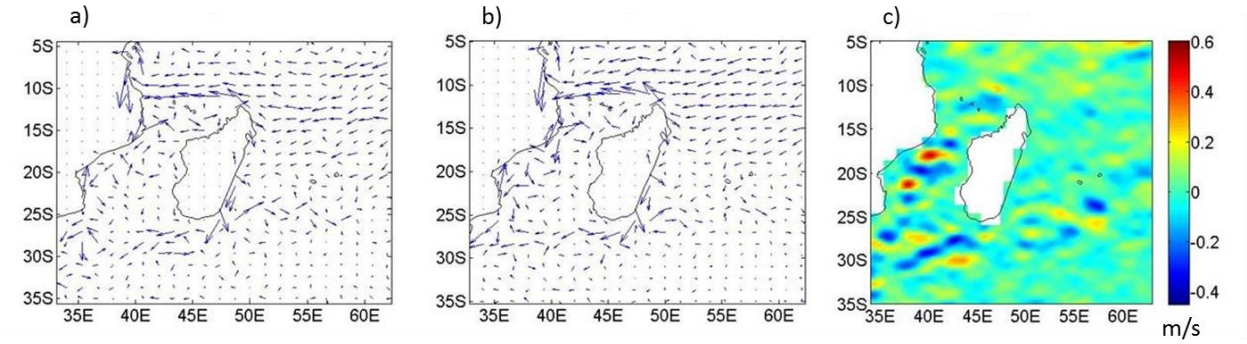

Figure 20. Composite maps of surface current vectors in a) bloom years, b) non-bloom years and c) the difference in the zonal component between bloom and non-bloom years. There are little monthly differences from December to March, so only March maps are shown here.

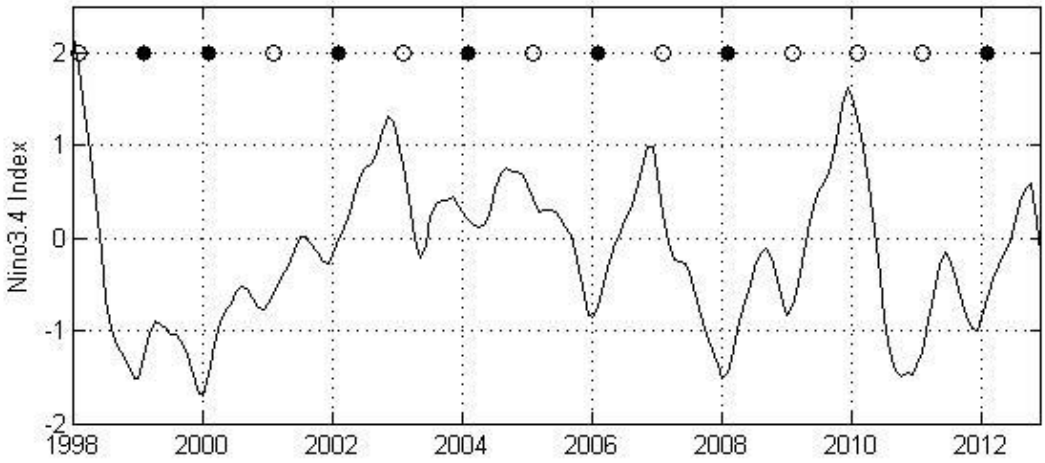

Figure 21. Niño3.4 index time series from 1998 to 2012. Solid circles mark bloom years and open circles mark non-bloom years for comparison.

Table 1: Datasets that will be used in this research, including variables, time period, and resolution of those datasets.

Dataset	Variable (units)	Time Period	Resolution
Sea-viewing Wide Field-of-view Sensor (SeaWiFS)	Chlorophyll Concentration (mg m^{-3})	1998-2009	1/12°x1/12°
Sea-viewing Wide Field-of-view Sensor (SeaWiFS)	Photosynthetically Active Radiation (E m^{-2} day^{-1})	1998-2010	1/12°x1/12°
Moderate Resolution Imaging Spectroradiometer (MODIS) – Aqua	Chlorophyll Concentration (mg m^{-3})	2003-2013	1/12°x1/12°
European Centre for Medium-Range Weather Forecasts (ECMWF) – ERA Interim	U- & V-components of surface wind (m s^{-1})	1979-2012	0.75°x0.75°
European Centre for Medium-Range Weather Forecasts (ECMWF) – ERA Interim	Surface Thermal Radiation (J m^{-2})	1979-2012	1.5°x1.5°
Tropical Rainfall Measuring Mission (TRMM)	Precipitation Rate (mm hr^{-1})	1998-2013	1/4°X1/4°
NOAA Geophysical Fluid Dynamics Laboratory (GFDL)	Mixed layer depth (db)	1961-2010	1°x1°
Ocean Surface Current Analyses – Real Time (OSCAR)	Surface Ocean Currents (m s^{-1})	1993-2013	1/3°X1/3°
Extended Reconstructed Sea Surface Temperature Version 3 (ERSSTv3)	Temperature (°C)	1870-2013	2°x2°
NASA Aquarius	Sea Surface Salinity (psu)	August 2011-present	1°x1°
Dipole Mode Index (DMI)	Index Anomaly (no units)	1958-2012	N/A
Niño3.4 Index	Index Anomaly (no units)	1950-2012	N/A

REFERENCES

Barnett, T.P. (1983). Interaction of the Monsoon and Pacific Trade Wind System at interannual time scales, Part I: The equatorial zone. *Mon Weath Rev*, 111, 756-773.

Conversi, A. & S. Hameed (1997). Evidence for quasi-biennial oscillations in zooplankton biomass in the subarctic Pacific. *J Geophys Res*, 102, 15659-15665.

DiMarco, S.F., Chapman, P., & W.D. Nowlin (2000). Satellite observations of upwelling on the continental shelf south of Madagascar. *Geophys Res Lett*, 27, 3965-3968.

Feng, M., & G. Meyers (2003). Interannual variability in the tropical Indian Ocean: a two-year time-scale of Indian Ocean Dipole. *Deep Sea Res., Part II*, 50, 2263-2284.

Grinsted, A., Moore, J.C., & S. Jevrejeva (2004). Application of the cross wavelet transform and wavelet coherence to geophysical time series. *Nonlinear Proc Geoph*, 11, 561-566.

Hansell, D.A. & R.A. Feely (2000). Atmospheric intertropical convergence impacts surface ocean carbon and nitrogen biogeochemistry in the western tropical Pacific. *Geophys Res Lett*, 27, 1013-1016.

Heywood, K.J., & Y.K. Somayajulu (1997). Eddy activity in the south Indian Ocean from ERS-I altimetry, Proceedings of 3rd ERS Symposium – Space at the service of our environment. Florence, Italy, ESA SP-414, 1479-1483.

Lutjeharms, J.R.E., & E. Machu (2000). An upwelling cell inshore of the East Madagascar Current. *Deep Sea Res, Part I*, 47, 2405-2411.

Lutjeharms, J.R.E. (2006). The ocean environment off southeastern Africa: a review. *S Afr J Sci*, 102, 419-426.

Longhurst, A. (2001). A major seasonal phytoplankton bloom in the Madagascar Basin. *Deep Sea Res, Part I*, 48, 2413–2422.

Machu, E., Lutjeharms, J.R.E., Webb, A.M., & H.M. Van Aken (2002). First hydrographic evidence of the southeast Madagascar upwelling cell. *Geophys Res Lett*, 29, 212009, doi:10.1029/2002GL015381.

McCreary, J.P., Kohler, K.E., Hood, R.R., & D.B. Olsen (1996). A four-component ecosystem model of biological activity in the Arabian Sea. *Prog Oceanogr*, 37, 193–240.

Meehl, G. A. (1993). A coupled air-sea biennial mechanism in the tropical Indian and Pacific regions: Role of the ocean. *J Clim*, 6, 31-41.

Meyers, G., McIntosh, P., Pigot. L., & M. Pook (2007). The years of El Niño, La Niña and interactions 6" with the tropical Indian Ocean. *J Clim*, 20, 2872-2880.

North, G.R., Bell, T.L., Cahalan, R.F., & F.J. Moeng (1982). Sampling Errors in the Estimation of Empirical Orthogonal Functions. *Mon Weather Rev*, 110, 699-706.

Poulton, A.J, Stinchcombe, M.C., & G.D. Quartly (2009). High numbers of *Trichodesmium* and diazotrophic diatoms in the southwest Indian Ocean. *Geophys Res Lett*, 36, L15610, doi:10.1029/2009GL039719.

Quartly, G.D. & M. Srokosz (2004). Eddies in the southern Mozambique Channel. *Deep Sea Res II*, 51, 69–83.

Raj, R.P., Peter, B.N., & D. Pushpadas (2010). Oceanic and atmospheric influences on the variability of phytoplankton bloom in the Southwestern Indian Ocean. *J Marine Syst*, 82, 217-229.

Hansell, D.A., & R.A. Feely (2000). Atmospheric intertropical convergences impacts surface ocean carbon and nitrogen biogeochemistry in the tropical Pacific Ocean. *Geophys Res Lett*, 27, 1013–1016.

Saji, N.H., Goswami, B.N., Vinayachandran, P.N., & T. Yamagata (1999). A dipole mode in the tropical Indian Ocean. *Nature*, 401, 260-363.

Saji, N.H., & T. Yamagata (2003). Possible impacts of Indian Ocean Dipole mode events on global climate. *Clim Res*, 25, 151-169.

Srokosz, M.A., Quartly, G.D., & J.J.H. Buck (2004). A possible plankton wave in the Indian Ocean. *Geophys Res Lett*, 31, L13301, doi:10.1029/2004GL019738.

Uz, B.M. (2007). What causes the sporadic phytoplankton bloom southeast of Madagascar? *J Geophys Res, 112*, C09010, doi:10.1029/2006JC003685.

Wilks, D.S. (2011). Statistical Methods in the Atmospheric Sciences: Third Edition. USA: Elsevier.

Yeo, S.R., & K.Y. Kim (2013). Global warming, low-frequency variability, and biennial oscillation: an attempt to understand the physical mechanisms driving major ENSO events. *Clim Dyn*, doi: 10.1007/s00382-013-1862-1.